the plant journal

SEB SOCIETY FOR EXPERIMENTAL BIOLOGY

The Plant Journal (2024) doi: 10.1111/tpj.16763

Multi-scale analysis of heat stress acclimation in Arabidopsis seedlings highlights the primordial contribution of energy-transducing organelles

Elise Réthoré[1,†], Sandra Pelletier[1], Thierry Balliau[2], Michel Zivy[2], Marie-Hélène Avelange-Macherel[1,*] and David Macherel[1,*]

[1]*Univ Angers, Institut Agro Rennes-Angers, INRAE, IRHS-UMR 1345, F-49000 Angers, France,*

[2]*INRAE, PAPPSO, UMR/UMR Génétique Végétale, Gif sur Yvette, France*

Received 9 October 2023; revised 8 March 2024; accepted 14 March 2024.

*For correspondence (e-mail david.macherel@univ-angers.fr; marie-helene.macherel@agrocampusouest.fr).

[†]Present address: Département R&D Nutrition Végétale, Centre Mondial d'Innovation du Groupe Roullier, Gestion des Stress Abiotiques chez les Plantes, 35400, Saint-Malo, France

SUMMARY

Much progress has been made in understanding the molecular mechanisms of plant adaptation to heat stress. However, the great diversity of models and stress conditions, and the fact that analyses are often limited to a small number of approaches, complicate the picture. We took advantage of a liquid culture system in which Arabidopsis seedlings are arrested in their development, thus avoiding interference with development and drought stress responses, to investigate through an integrative approach seedlings' global response to heat stress and acclimation. Seedlings perfectly tolerate a noxious heat shock (43°C) when subjected to a heat priming treatment at a lower temperature (38°C) the day before, displaying a thermotolerance comparable to that previously observed for Arabidopsis. A major effect of the pre-treatment was to partially protect energy metabolism under heat shock and favor its subsequent rapid recovery, which was correlated with the survival of seedlings. Rapid recovery of actin cytoskeleton and mitochondrial dynamics were another landmark of heat shock tolerance. The omics confirmed the role of the ubiquitous heat shock response actors but also revealed specific or overlapping responses to priming, heat shock, and their combination. Since only a few components or functions of chloroplast and mitochondria were highlighted in these analyses, the preservation and rapid recovery of their bioenergetic roles upon acute heat stress do not require extensive remodeling of the organelles. Protection of these organelles is rather integrated into the overall heat shock response, thus allowing them to provide the energy required to elaborate other cellular responses toward acclimation.

Keywords: acclimation, chloroplast, heat, heat shock response, mitochondria, organelle, photosynthesis, priming, respiration.

INTRODUCTION

Climate change has now become a manifest threat to plant growth and development. The occurrence of stronger and longer heat waves over the past years has already led to severe reductions in crop yields (Ciais et al., 2005; Perkins-Kirkpatrick & Lewis, 2020; Zampieri et al., 2017). Even though the impact of heat stress on plants has been studied for decades and regularly reviewed (Bita & Gerats, 2013; Fahad et al., 2017; Hatfield & Prueger, 2015; Jagadish et al., 2021; Kan et al., 2023), the understanding of plant heat stress tolerance is still incomplete. High temperatures were shown to cause damage at the molecular level, such as protein and membrane destabilization, which in turn disturbs the proper functioning of plant physiology and metabolism (Niu & Xiang, 2018; Ruelland & Zachowski, 2010). The photosynthetic activity appears to be rapidly affected under heat stress: the thylakoid membranes become unstacked, and the activity of photosystem II is disrupted, which causes an imbalance in photosynthesis and contributes to reactive oxygen species accumulation (Allakhverdiev et al., 2008; Mathur et al., 2014). Although mitochondria are known to better tolerate heat stress compared to chloroplasts, respiration also declines when reaching temperatures over 45°C (Atkin & Tjoelker, 2003; Hüve et al., 2011; Scafaro et al., 2021). To counteract the negative effect of high temperatures on their physiology and metabolism, plants have evolved

mechanisms of thermotolerance, described as the "heat stress response (HSR)", which has been extensively investigated over the past decades (Ohama et al., 2017). The HSR is known to be triggered by several primary signals, including Ca^{2+} import via cyclic nucleotide-gated calcium channels (CNGC), protein destabilization, and ROS signaling (Driedonks et al., 2015; Finka et al., 2012; Mittler et al., 2012; Richter et al., 2010; Saidi et al., 2011; Volkov et al., 2006). However, temperature sensing by plants appears as a far more complex and intricate array of mechanisms that includes photoreceptors and circadian clock components, in which biophysical transitions within membranes and proteins could play critical roles (Hayes et al., 2020). Through multiple cascades of signal transduction (including calmodulins, unfolded protein response, and epigenetic modifications), these early events lead to the expression and activation of the transcriptional HSFs (heat shock factors) and DREBs (dehydration-responsive elements-binding factors), which drive the expression of heat shock proteins (HSPs), including chaperones, ROS-detoxifying enzymes (ascorbate peroxidase, catalase) and others (Ohama et al., 2017). Chaperones are members of several conserved families of HSPs (HSP20, HS40, HSP60, HSP 90, HSP100) that control cellular proteostasis. The fact that several members are highly overexpressed upon heat stress has led to their annotation as HSPs, although their majority is expressed constitutively (Finka et al., 2016). Under stress and recovery, chaperones are involved in the prevention of protein (and RNA) aggregation and the disaggregation of cytotoxic aggregates and unfolding of misfolded proteins, but also in the protection of membranes (Allakhverdiev et al., 2008; Finka et al., 2016; Liberek et al., 2008; McLoughlin et al., 2016; Richter et al., 2010). Even though much is known about the structure of chaperones and their unfoldase functions, their precise role in the different cellular compartments is still unclear. In plants, the small HSP (sHSP) family has expanded with for instance 18 members in Arabidopsis, which are distributed in the cytosol, nucleus, plastid, mitochondrion, endoplasmic reticulum, and peroxisome (Waters & Vierling, 2020). For most of them, gene expression is strongly inducible by heat stress in vegetative tissues or under developmental control in seeds and pollen (Siddique et al., 2008). In the mitochondrion, sHSPs were shown to preserve the activity of complex I upon stress and to participate in protein protection against heat denaturation, as recently shown for the pea mitochondrial HSP22 (Avelange-Macherel et al., 2020; Downs & Heckathorn, 1998; Hamilton III & Heckathorn, 2001). In the chloroplast, HSP21 was shown to play a role in the maintenance of photosynthesis by stabilizing photosystem II subunits and protecting an RNA-polymerase (Chen et al., 2017; Zhong et al., 2013). Besides the role of this sHSP, it was recently demonstrated that the chloroplast was a key player in heat stress signaling for the acquisition of thermotolerance (Chen et al., 2017; Dickinson et al., 2018; Sun & Guo, 2016). However, even if the effects of heat stress on chloroplast metabolism have already been explored, the mechanisms of energy metabolism protection need to be further investigated (Wang et al., 2018).

During the early life of plants, the seedling stage is considered stress-sensitive, even though it is usually transient in many species (Leck et al., 2008). In particular, the efficiency of both respiration and photosynthesis at the early seedling stage is critical for ensuring the transition from seed reserve mobilization to photo-autotrophy. However, despite their fragile appearance, seedlings need to be competitive and resilient to assume the change from a highly stress-tolerant seed to an established plant, which can allocate resources to growth and stress responses. In previous work, we have shown that Arabidopsis seedlings maintained in liquid culture could survive for weeks under severe mineral starvation, thanks to the arrest of their development and their metabolic plasticity (Réthoré et al., 2019). By balancing their energy metabolism through high alternative oxidase and photorespiratory activities, they could remain self-sufficient and fully viable for weeks, resuming their normal development upon transfer to the soil. This experimental model is well suited to study the response and acclimation of seedlings to environmental stress such as heat for several reasons. First, homogenous populations of thousands of seedlings can be subjected to accurate heat regimes without interference with drought stress since all experiments are done in a liquid medium. Second, because seedlings are arrested in their development, the model allows studying the effect of stress treatments on physiology and metabolism without interference with developmental effects, which often hampers proper comparisons between stress and control samples. We, therefore, took advantage of this robust experimental system to perform a multi-scale analysis of heat acclimation of Arabidopsis seedlings, combining omics with functional analyses of mitochondria and chloroplasts. The overall results highlighted the role of HSPs and demonstrated that protection and rapid recovery of energy metabolism upon heat stress was decisive for successful acclimation to a severe heat shock.

RESULTS

Priming allows seedling survival after heat shock

We established an experimental model in which 7-day-old seedlings could survive a lethal heat shock (H) thanks to a pre-treatment (priming, P) at a lower temperature 24 h before. We selected a stress duration of 2 h for both treatments, with P applied at 38°C on day 6 of growth and H at 43°C on day 7 (Figure 1a). A low light intensity comparable to that of the growth room was applied during the different treatments to prevent any effect of darkness on heat stress response (Caldana et al., 2011; Song et al., 2016). In these conditions, the P treatment alone did not affect seedling

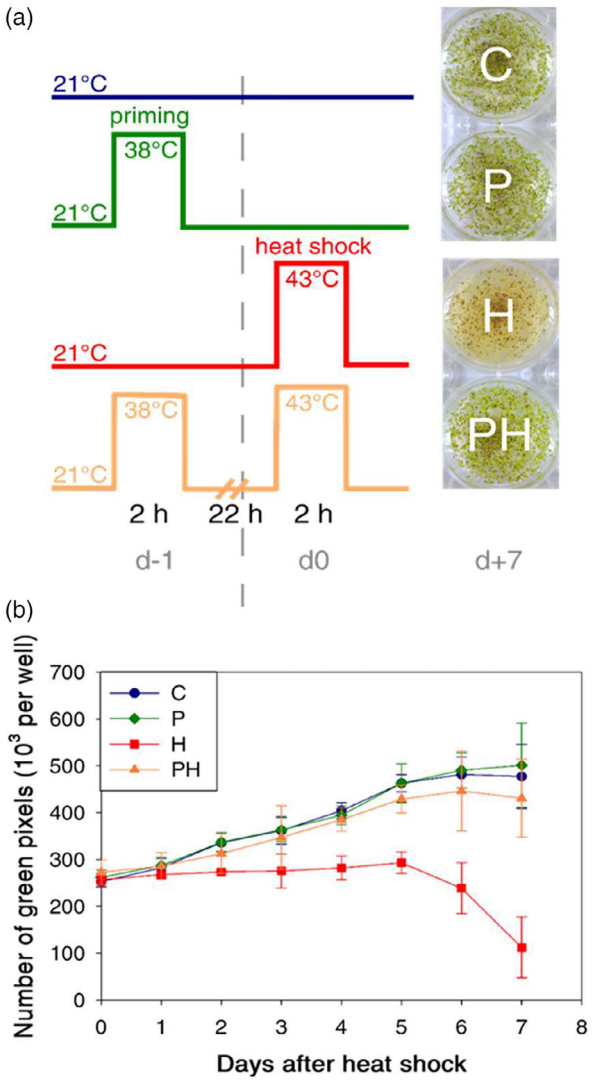

Figure 1. Heat stress regimes and seedling thermotolerance.
After six or 7 days of culture in six-well plates (d−1 or d0, respectively), seedlings and their medium were transferred into 25 ml glass containers and placed in a water bath (38 or 43°C) in the presence of light (150 μmol photons.m^{-2}.sec^{-1}, growth light intensity). After treatment, seedlings were transferred back into the six-well plates for recovery. C: control; P: priming; H: heat shock; PH: priming + heat shock. (a) Heat stress regimes and representative pictures of wells on day 14 (7 days after 43°C treatment). (b) Quantification of green pixels in the wells during the days following 43°C treatment ($4 < n < 11$).

survival, whereas the H treatment triggered the death of the seedlings, which was scored after 7 days of recovery. When both treatments (priming + heat shock, PH) were combined, the seedlings were fully protected against the otherwise lethal heat shock (Figure 1a). These results were comparable to previous studies performed on agar plates (Halter et al., 2017; Kang et al., 2016; Queitsch et al., 2000), indicating that liquid-grown seedlings display classical heat shock and acclimation responses. To quantify the effect of the treatments on the seedlings, we measured the number of green pixels per well during the 7 days following the H treatment (Figure 1b). In C, P and PH conditions, the number of green pixels per well increased two-fold during the 7 days after treatment, which is due to the expansion of cotyledons (Réthoré et al., 2019). Although there is a slight reduction in the green pixels for PH samples, it is not statistically significant, which confirms that priming has no effect on late seedling development and fully protects from the noxious heat shock. Indeed, in H wells, the green pixel amount was stable until 5 days after stress and progressively decreased after that, reflecting the subsequent loss of chlorophyll and seedling death. From 2 days after heat shock, the number of pixels was significantly lower in H compared to C. It is noticeable that the decrease was slow, and the death occurred around 6 days after treatment, possibly through programmed cell death. Altogether, these data reveal that developmentally arrested seedlings developed a classical acquired thermotolerance and thus constitute an excellent material to study heat stress acclimation.

Full and rapid recovery of energy metabolism after heat shock is correlated with seedling survival

We next examined the impact of heat stress on respiration and photosynthesis, which are the main drivers of energy metabolism for seedlings. Respiratory and photosynthetic activities were measured by oxygraphy, at 43°C just after heat shock, and then at 25°C during the recovery period (Figure 2). After 2 h at 43°C, dark respiration and net photosynthesis in PH samples were 1.5 times higher than in H samples, indicating that priming significantly protected photosynthesis and respiration during the heat shock at 43°C. Regarding the evolution of respiration and net photosynthesis during the recovery period, respiration measured at 25°C for the non-treated samples (C, control) decreased around two folds from day 0 to day 4 and then stabilized, while photosynthesis remained stable (around 40 nmol O_2 sec^{-1} mg^{-1} chll) (Figure 2c,d). P seedlings displayed similar values to the control, confirming that the priming treatment is innocuous for the seedlings, with no long-term effect on energy metabolism and viability. On the contrary, H seedlings displayed lower activities that were markedly and irreversibly affected from 2 h of recovery (Figure 2c,d): net photosynthesis was 36% lower than the control after 2 h of recovery and further decreased when the seedlings were progressively dying, while dark respiration remained stable during the days following treatment. The increase in respiratory rate after 6 days is simply due to the loss of chlorophyll (used as a reference) of the dying seedlings.

Interestingly, heat shock had a more substantial impact on respiration than on photosynthesis after 2 h of recovery, although photosynthesis is usually considered the most sensitive component to heat stress (Mathur et al., 2014; Posch et al., 2019; Wahid et al., 2007; Yamori et al.,

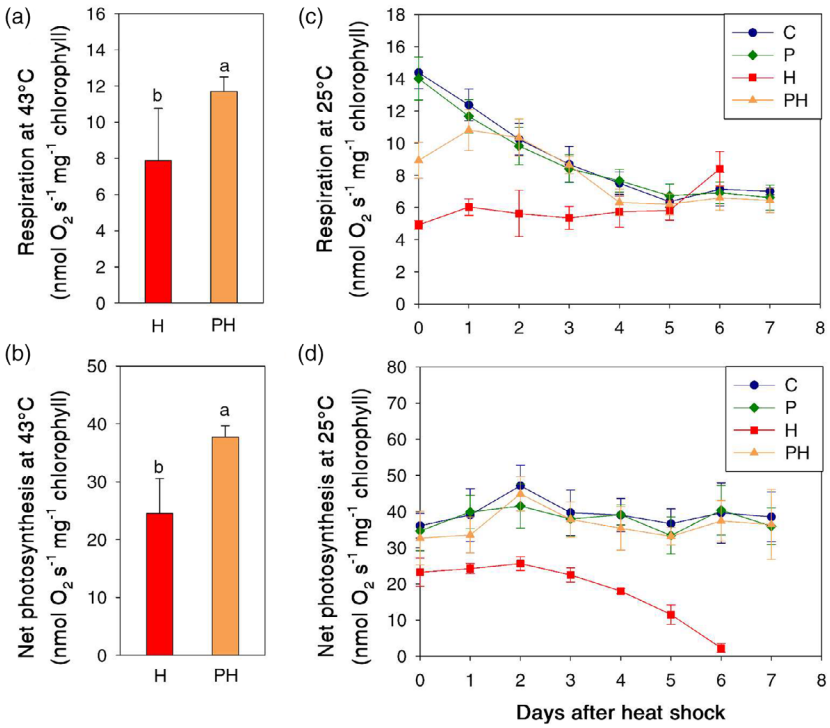

Figure 2. Impact of heat stress on respiratory and net photosynthetic activities.
Dark respiration and net photosynthesis at 800 μmol photons.m^{-2}.sec^{-1} were acquired by oxygraphy. Seedlings were placed for 2 h at 43°C (H, PH) and directly transferred into the electrode calibrated at the same temperature for measurement of dark respiration (a) and net photosynthesis (b) (n = 8). In a second experiment, seedlings were transferred back into the growth room after stress and dark respiration (c) and net photosynthesis (d) were measured in the electrode calibrated at 25°C after 2 h of recovery (day 0 after heat shock) and on the following days (n = 6). C: control; P: priming; H: heat shock; PH: priming + heat shock. The bars indicate SD of the mean. Letters denote significant differences according to ANOVA and Tukey test (P < 0.05).

2014). This is likely due to the mid-term adaptation to heat shock and recovery on these two components, compared to the short and acute heat stress or prolonged and moderate heat stress effects observed in other studies (Hüve et al., 2011; Wang et al., 2020). It could also result from a different regulation of shoot and root respiration, measured together in our measurements. In PH seedlings, dark respiration, and net photosynthesis were lower (9 and 33 nmol O_2 sec^{-1} mg^{-1} chll, respectively) than those of C seedlings (14 and 36 nmol O_2 sec^{-1} mg^{-1} chll, respectively) when measured 2 h after stress, but higher than those of H seedlings (5 and 23 nmol O_2 sec^{-1} mg^{-1} chll, respectively). After 1 day of recovery, dark respiration and net photosynthesis of PH seedlings were like the control, which confirms the effectiveness of priming in protecting energy metabolism. We also performed chlorophyll fluorescence imaging to analyze the effect of priming and heat shock on photosystem II maximum quantum yield (Fv/Fm). A value of around 0.8 is considered a standard for healthy plants, whereas lower values are observed in stressed plants (Baker, 2008). Just after the 43°C heat shock, the Fv/Fm of the H seedlings was much lower (0.61) than those of the C or P samples (0.82), while that of the PH sample decreased to 0.67 (Figure S1). Complete recovery of the Fv/Fm value of the PH sample was observed after 1 day of recovery, while the H seedlings Fv/Fm value decreased further. Collectively, these results reveal that priming has a major beneficial effect on seedlings' energy metabolism during heat shock and recovery. Moreover, it is even possible to predict whether seedlings will ultimately die or survive based on oxygraphic measurements acquired during heat shock or after 2 h of recovery, which highlights the importance of energy metabolism in heat stress tolerance.

Priming allows the recovery of organelle dynamics after heat shock

Mitochondria are highly motile organelles that use the actin network to move on (Van Gestel et al., 2002). Mitochondrial dynamics was previously identified as a component of cell death, and heat shock was shown to trigger an abnormal mitochondrial morphology in protoplasts (Logan, 2010). Given the protection of respiratory activity induced by priming in PH seedlings, we wondered if priming could influence the response of mitochondrial dynamics to heat shock. For this purpose, we used a transgenic line expressing green fluorescent protein targeted to mitochondria (Mito-GFP line), which was subjected to different heat treatments and observed by wide-field epifluorescence microscopy.

Time-lapse acquisition of fluorescence throughout 20 sec in cotyledon cells allowed us to examine mitochondrial motility by particle tracking (Figure 3). Speed per track analyzed just after priming was highly variable for both C and P seedlings, with values from 0.2to 2.8 μm sec^{-1}, reflecting the heterogeneity of mitochondrial dynamics. The mean speed per track was around 110 nm sec^{-1} for C seedlings and 125 nm sec^{-1} for P seedlings just before heat shock. After heat shock, for both H and PH seedlings, the mean speed of mitochondria dropped to 7.2 and 6.1 nm sec^{-1}, respectively. Thus, heat shock strongly affected mitochondrial motility, even in the case of primed seedlings. However, after 24 h of recovery, PH seedlings recovered a mean mitochondrial speed of 95 nm sec^{-1}, whereas in the H condition, mitochondrial motility remained low (8.2 nm sec^{-1}). Mitochondrial dynamics in PH seedlings fully recovered within 8 h after heat shock, as shown in Figure S2. The capacity of primed seedlings to survive a heat shock is therefore correlated to the rapid recovery of energy metabolism and mitochondrial dynamics. In contrast, in H seedlings, the absence of recovery of mitochondrial dynamics might be an early indicator of cell death establishment, as was previously shown in protoplasts (Scott & Logan, 2008). Under these conditions, the inability of mitochondria to move and fuse to exchange DNA, proteins, or metabolites could seriously impair their function and maintenance.

We used a transgenic line expressing an ER-targeted GFP protein to check whether the movements of the endoplasmic reticulum (ER), another motile sub-cellular compartment, were impacted by heat shock. The dynamics were quantified by computing the Pearson's correlation coefficient for co-localization of the fluorescence between two images acquired 20 sec apart, with measured values of 0.80 for both C and P seedlings before heat shock (Figure S3). A blockage of ER dynamics just after heat shock was evident in both H and PH conditions since Pearson's correlation values were close to 1. However, while ER dynamics remained blocked in H seedlings after 24 h, it was already well restored in PH seedlings with a value of 0.86. Therefore, it is likely that the effects of heat shock and priming on mitochondrial dynamics are not specific to the organelle. As movements of mitochondria and ER depend on the actin network in plants (Perico & Sparkes, 2018), we hypothesized that the impact of heat shock and priming on these organelle dynamics was primarily due to an effect on the actin microfilament network. Indeed, heat shock was previously shown to cause cytoskeleton depolymerization and disassembly (Fan et al., 2016; Malerba et al., 2010; Müller et al., 2007), but the effect of priming was not studied. We thus performed a similar analysis using a line expressing a GFP targeted to the actin microfilaments (Lifeact-GFP). Since it was more challenging to distinguish actin filaments by epifluorescence microscopy clearly, we observed the GFP-labeled actin

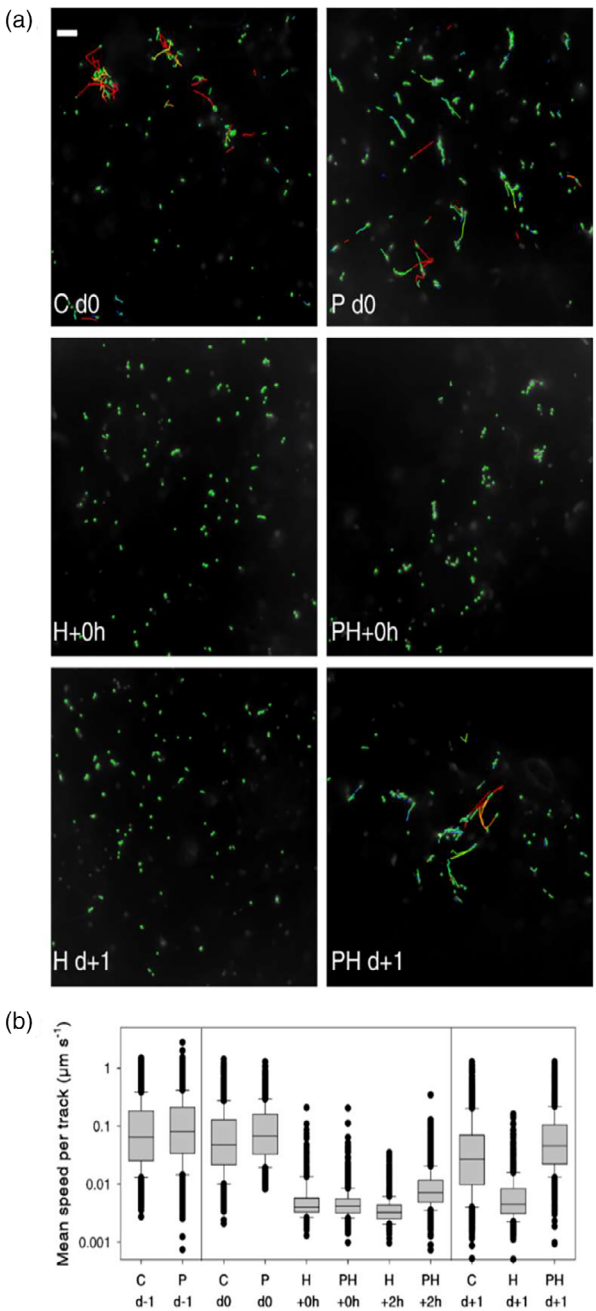

Figure 3. Evolution of mitochondrial dynamics in response to heat stress. Seedlings expressing mitochondrial GFP (Mito-GFP line) were observed by wide-field epifluorescence microscopy.
(a) Images generated using Imaris software to track mitochondria in cotyledon cells over a period of 20 sec. Detected mitochondria are green colored and tracks are rainbow colored according to mean speed (no movement is purple, and movement above 0.5 μm/sec is red). Each image is representative of data captured from at least three independent seedlings and two technical replications per seedling. Bar = 5 μm. C: control; P: priming; H: heat shock; PH: priming + heat shock.
(b) Boxplots of the mean speed recorded per track in micrometers/second according to tracking using Imaris software. Total number of tracks analyzed per time point ranges from 536 to 4442. Imaging was performed just after priming (d−1), just before heat shock (d0), after heat shock (+0 h), after 2 h of recovery (+2 h) or after 24 h of recovery (d+1).

network using laser scanning confocal microscopy (LSCM). Sequential acquisition of two images 2 min apart allowed computing the extent of co-localization of the fluorescence via Pearson's correlation coefficient as an indicator of actin microfilament motility (Figure 4). The Pearson's coefficient values close to 0.92 observed in H and PH samples after heat shock reflect the arrest of actin microfilament movement, compared to values close to 0.5 observed in C and P conditions, in which the actin cytoskeleton is highly dynamic. As observed for mitochondria and ER dynamics, the full recovery of actin dynamics in PH seedlings occurred within 1 day after heat shock, but no recovery occurred in the case of H seedlings. Altogether, these observations reveal that priming itself does not prevent the arrest in actin network dynamics occurring during heat shock. However, a fast recovery is observed in primed samples, which allows organelles such as mitochondria and ER to rapidly resume their normal dynamics after a period of blockage triggered by high temperature. Protective mechanisms such as interaction with sHSPs could contribute to the rapid resumption of actin dynamics since these proteins were shown to interact with actin in mammal cells (Mounier & Arrigo, 2002). In H seedlings, the loss of actin cytoskeleton dynamics could affect that of other organelles such as mitochondria and ER, compromising their functions and contributing to the signaling toward induction of programmed cell death.

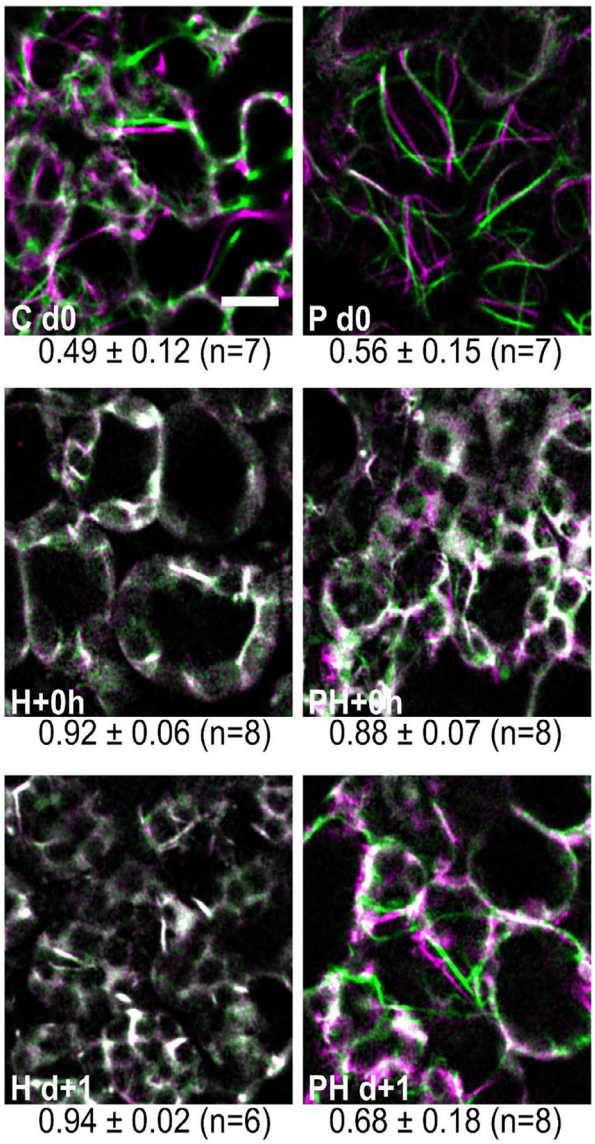

Figure 4. Evolution of Actin dynamics in response to heat stress.
Seedlings expressing GFP targeted to the Actin network (LifeAct-GFP line) were observed by laser confocal scanning microscopy. Merged images of two frames captured 2 min apart in cotyledon cells are shown; the first image was false-colored in green and the second in magenta; co-localization corresponds to white pixels. Data were captured from at least 3 independent seedlings and 2 technical replications per seedling. Values below the images correspond to the mean of Pearson's correlation coefficient ± SD. The coefficient was calculated using Fiji Coloc 2 colocalization tool. Scale bar: 10 μm. C: Control; P: Priming; H: Heat shock; PH: Priming + heat shock. Imaging was performed just before heat shock (d0), after heat shock (+0 h) or after 24 h of recovery (d+1).

Primed seedlings exhibit a specific transcriptional response under heat shock

A multi-omics approach was started to characterize further seedlings' response to priming and heat shock at the molecular level. Since the transcriptome is known to respond quickly to heat (Larkindale & Vierling, 2007), we first analyzed the early transcriptional responses after 30 min of priming (P sample) or heat shock (H and PH samples), in comparison to control condition C (before priming). Using the RNA-seq strategy, including ribosomal RNA depletion for library construction, allowed analyzing the expression of all mRNAs, including those from organellar transcriptomes. Sequencing data comprised between 8.3 and 17.1 billion clean bases for each sample, allowing a coverage between 30 and 63×. For differential analysis, sense transcripts with a minimum fold change of 2 and a false discovery rate of less than 0.05 were considered as significantly differentially expressed (DE) between the two conditions (Table S1). We detected 3883 transcripts significantly upregulated and 4075 downregulated in at least one condition. Figure 5a,b shows the number of DE transcripts for each temperature treatment, compared to C. The total number of downregulated transcripts was lower in the H condition than in P or PH. The number of upregulated transcripts was higher in PH than in the other treatments. A core response of 406 upregulated genes and 342 downregulated genes was found in all heat treatments. Among the gene ontologies (GO) related to these upregulated genes figured: "response to heat stress", "response to high light intensity", "response to oxidative stress", "transcription activator activity", and "protein folding". Genes previously identified as main actors of the HSR were

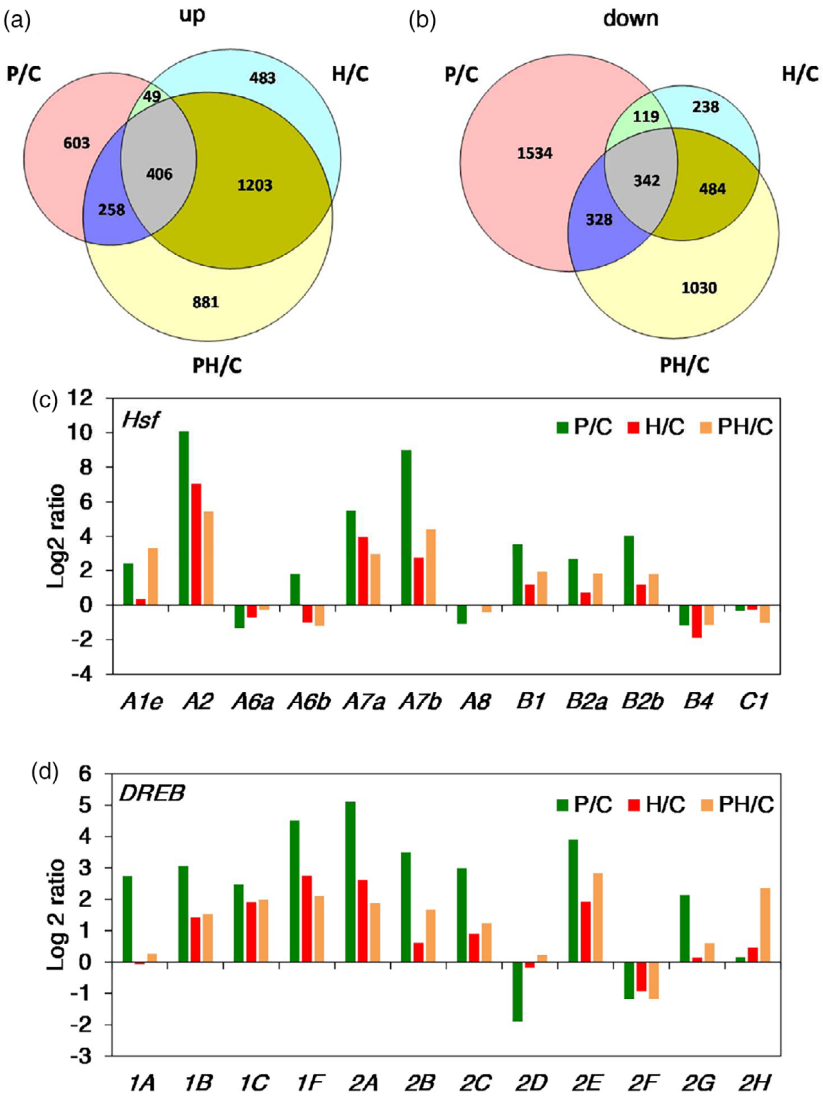

Figure 5. General transcriptional responses to priming and heat shock and regulation of major transcriptional factors Hsf and DREB.
Venn diagrams representing the number of significantly upregulated (a) and downregulated (b) transcripts in response to the different heat stress regimes (FDR <0.05 and log2 ratio >1 or <−1). Data were acquired before priming (C) or after 30 min of the different stress applications (P, H and PH). Log2 ratio of Hsf and DREB transcription factors whose expression was significantly affected by at least one treatment are shown in (c) and (d), respectively.

detected among the most upregulated genes in all treatments, even if, for most of them, the fold change was often lower in H than in P and PH. For example, among the transcription factors, *HSFA2*, *HSFA7a*, *HSFA7b*, *HSFB1*, and *HSFB2b* genes were found to be upregulated in all conditions, as well as those for DREB factors 1B, 1C, 1F, 2A, and 2E, but the response was lower in H condition compared to P (Figure 5c,d). Interestingly, most of these genes were not expressed to a higher level in PH compared to the H condition, although the PH seedlings survive, while the H seedlings are committed to death. Regarding the common downregulated genes, the main GO associated were: "response to auxin", "carbohydrate metabolic process", "cell wall organization", and "lignin catabolic process". The core response (342 transcripts) involved many auxin-responsive genes (SAUR), a few ethylene-responsive transcription factors (ERF, CRF and LEP), many cell-wall-related enzymes (polygalacturonase, expansins, cellulose synthase, pectin acetylesterases…). All these data fit with an early response associated with the arrest of growth and development. Overall, these results agree with previous studies of heat stress signaling (Ahuja et al., 2010; Lim et al., 2006; Ohama et al., 2017) and validate our experimental system. When comparing the different conditions to control C, we found that 75% of significantly upregulated transcripts in the H condition were also upregulated in the PH condition, while only 21% of upregulated transcripts in H were shared with the P condition. In total, 50% of genes upregulated in P were also upregulated in PH condition. The transcriptome of PH seedlings thus comprises a high overlap with those of P and H seedlings. We will thereafter focus on the DE genes specific to P and/or PH, which are thus candidates for a role in basal and acquired thermotolerance. The common response to P and PH treatments included 258 upregulated transcripts and 328 downregulated transcripts (Figure 5a,b). The overexpressed genes

were identified in the gene ontologies (GO) related to "response to heat" and "protein folding" and encoded for two HSP70, three HSP40-like proteins, two chaperonins 60 and three FKBP peptidyl-prolyl cis-trans isomerases. Other transcripts such as *HSFA1e*, *HSFB2a*, *DREB2B*, *DREB2C* (Figure 5c,d), *ERF021*, and several transcripts encoding glutaredoxins were also part of this common response. The downregulated transcripts were linked to "cell wall modification", "protein phosphorylation", "protein tyrosine kinase activity", and "aspartic-type endopeptidase activity" GOs. Regarding the DE transcripts specifically responding to PH treatment, 881 were specifically upregulated, and 1030 were specifically downregulated (Figure 5a,b). The GOs related to this specific response in PH seedlings compared to the other treatments are shown in Figure 6. Interestingly, the major GOs linked to cellular components specifically upregulated in PH comprised "plastid", "cytoplasm", and "mitochondrion". "Photosynthesis", "pigment biosynthetic process", and "response to oxidative stress" were the most represented biological processes GOs among the upregulated transcripts (Figure 6a). In contrast, a high number of decreased transcripts were identified in the "cell wall modification" or "response to salicylic acid" or "microtubule" GOs (Figure 6b). As suggested by (Larkindale & Vierling, 2007), the efficient downregulation of genes that are not required for heat stress tolerance or could be damageable for the plant is likely required in the process of thermotolerance.

Among the 881 PH-specific upregulated genes, 151 (17%) were predicted to encode plastidial proteins according to SUBA4. They were linked to "photosynthesis" (photosystem II proteins, chlororespiration reduction 1 (*CRR1*), phosphoglycerate kinase 1, early light-induced protein 1), "protein folding" (*CpHSC70-1*, chaperonin 60-alpha, a putative HSP10), chlorophyll metabolic process (biosynthesis), "cellular amino acid biosynthetic process" (Phe, Leu, Tyr, Lys, and Cys biosynthesis) or "ribosome biogenesis and translation" GO (50S, 30S and S21 ribosomal proteins, an elongation factor P (EF-P) family protein, chloroplast ribosome release factor 1 (*CPRF1*) and *CSP41A* involved in rRNA maturation) (Table S1). Furthermore, among the transcripts predicted to encode mitochondrial proteins, 63 were overexpressed specifically in PH (representing 7% of PH-specifically upregulated transcripts). Nine encoded PPR proteins and one MORF3 (multiple organellar RNA editing factor 3) could reflect a specific regulation of RNA editing in the mitochondrion. Thus, PH seedlings exhibited a differential response of the genes encoding plastidial or mitochondrial proteins compared to the H condition, which may contribute to their heat stress tolerance.

Since there were significant differences between the responses of H and PH seedlings at the level of energy metabolism, we scrutinized the transcriptional response of nuclear and organellar genes encoding components of the photosynthetic and respiratory electron transport chains (Figure 7). Most of the photosynthesis-related genes were overexpressed in P samples after 30 min of treatment (89 out of 109 transcripts significantly upregulated) (Figure 7). Among them, nine had a fold-change >2 (log2 > 1), and five of them were coding proteins of photosystem II (psbA, psbB, psbC, psbD, psbE). This increase could be related to a higher turnover of photosynthetic components at 38°C compared to 25°C. Regarding the genes overexpressed in response to 43°C treatment, several genes were specifically upregulated in PH condition (compared to H), in particular those encoding subunits involved in the NAD(P)H dehydrogenase complex (NdhL, NdhN, NdhO, NDF2, NDF4, NDF6) (Figure 7). We could also identify several photosystem I and photosystem II subunits (PsaD1, PsaH2, Psal, PsbS) among the PH-specifically overexpressed genes. In the mitochondrion, 89 out of 106 transcripts corresponding to both mitochondrial and nuclear genes were also significantly upregulated in the P condition, possibly contributing to sustaining the high respiration at 38°C. In contrast, in H and PH samples, the upregulated transcripts mainly consisted of mitochondrial-encoded transcripts, which could reflect a disturbance of the organelle/nucleus transcriptional regulation. Regarding the genes involved in mitochondrial dynamics, we could not detect any significant changes in their transcription, except the upregulation of *DRP1E* (AT3G60190.1) in the P condition and the downregulation of *DRP5A* (AT1G53140.1) in the PH condition, both encoding dynamin-related proteins (Table S1). The actin-related protein C2B transcript was also downregulated in both H and PH conditions. This indicates that the changes observed in mitochondrial dynamics were not due to a transcriptional response at this level.

We finally performed a sparse variant of the PLSDA (sPLS–DA) to determine the subsets of genes that best discriminate the four samples (C, H, P, PH) and could stand for heat tolerance markers. Three components composed of 10, 60, and 30 genes, respectively, were identified (Table S2). As shown in Figure S4, the first component of the optimized model explained 46% of the variance in gene expression level and discriminated perfectly with the control condition. The ten discriminative genes were all downregulated in P, H, and PH compared to the control. They were related to cell wall organization and metabolism as indicated by Gene Ontology. This result suggests that non-lethal and lethal heat stress may affect cell wall homeostasis. The second component explained 28.2% of the variance in gene expression levels and discriminated well with the P condition. Among the 60 selected variables were found upregulated transcripts of heat shock proteins and downregulated transcripts of PPR proteins. Genes were mostly related to protein folding and response to stress, as indicated by Gene ontology (Figure S4). However, the first two selected transcripts were encoding a

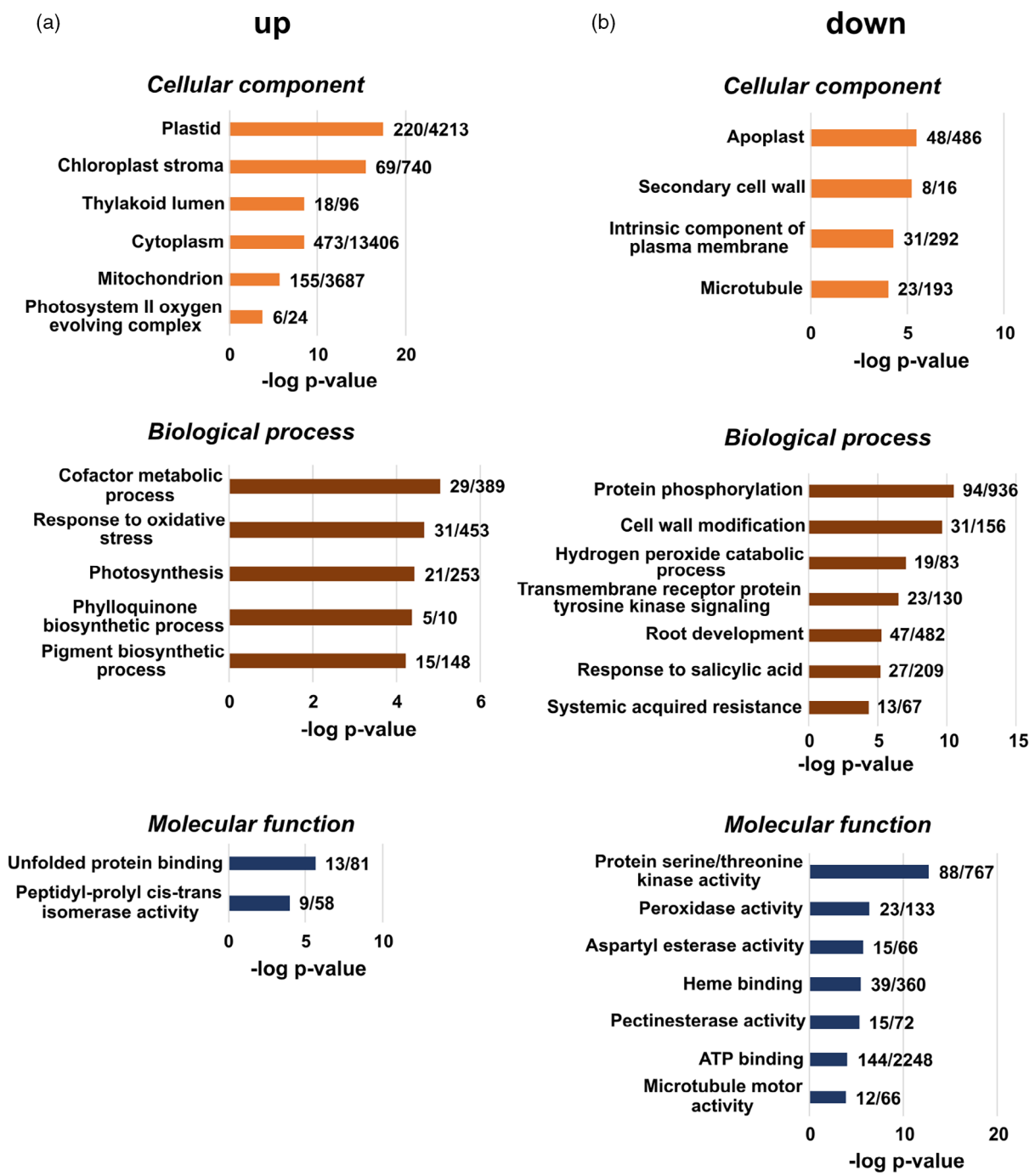

Figure 6. Gene ontology of transcripts specifically responding to PH treatment.
−Log *P*-values were calculated based on the gene ontology from AgriGO v2 of PH specifically upregulated or downregulated transcripts (FDR <0.05; log2 ratio >1 or <−1). The most significant categories ($P < 0.0005$) were represented for each component.

putative glycosyl transferase (AT3G10630.1, downregulated in P) and a cycling DOF factor 1 (AT5G62430.1, upregulated in P). The latter protein is involved in relation to TOPLESS in transcription repression. The third component explained 11.1% of the variance in gene expression level and discriminated PH from H. Selected genes were regulated in opposite ways in H and PH: those that were downregulated in H were upregulated in PH and vice-versa. However, no pertinent connection could be found among these 30 selected genes using Gene Ontology. The first selected gene *AT3G21720.1*, which was upregulated in PH, encodes isocitrate lyase, a key enzyme in

the glyoxylate cycle. This pathway plays an important role during seed germination by converting stored-lipids into available carbon source but might also contribute to stress tolerance by modulating energy metabolism (Yuenyong et al., 2019). However, the transcript encoding malate synthase, the other key enzyme of the pathway, was downregulated in the PH condition (Table S2).

Altogether, these transcriptomic data revealed the upregulation of several heat-stress responsive genes (*HSF*, *HSP*) and photosynthesis-related genes in the PH condition compared to the H condition, which could contribute to better maintenance of energy metabolism under and after heat shock.

Comparative proteomics reveals complementary profiles for priming and heat shock

Since transcriptional responses are not necessarily correlated with changes at the protein level, particularly under stress conditions (Kosová et al., 2011), we also analyzed the heat shock response using shotgun proteomics. The highly sensitive XIC method (Belouah et al., 2019) was used to determine the abundance of the proteins in the different conditions: C and P (22 h after priming), H and PH condition (2 h of recovery post-heat-shock). Among the 4544 proteins identified, 740 were retained for quantification after data filtration. Of these, 266 proteins significantly accumulated, and 143 proteins decreased in at least one treatment compared to the control condition (Figure 8 and Table S3). When applying thresholds for variation (ratio >2 or <0.5), 118 proteins (44% of the total) accumulated more than twice, and 65 proteins (45% of the total) decreased by more than half. Although this corresponds to a 45% overall proportion of proteins displaying high up or down variation, the Venn diagram shows that the proportion strongly depends on the conditions (Figure 8). Hence, among the nine proteins accumulating or the 14 proteins decreasing in all three conditions (P, H, PH), only one protein displayed a strong up or down variation. Interestingly, the highest number of differentially accumulated proteins was observed following heat shock, with considerable overlap between H and PH conditions (44.7% of total increased and 40.6% of total decreased proteins). Another noticeable observation is the fact that we did not detect any protein significantly accumulating or decreasing exclusively in both P and H conditions, while many proteins were found to respond specifically to both P and PH or H and PH conditions (Figure 8). This highlights the potency of the 43°C noxious heat shock on the seedling proteome but also shows that proteome response in the PH samples is shaped by the successive impacts of priming and heat shock, although these treatments, when not combined, have different impacts, and consequences (life or death).

Proteomic data were first analyzed by STRING (Szklarczyk et al., 2019) in order to highlight potential protein clusters up and downregulated in P, H, and PH conditions compared to control. The list and composition of clusters are presented in Table S4, while Figure 9 shows the network views of the main clusters identified for each condition. Cluster comparisons were performed according to the description of the cluster and its protein members, but it should be noted that clusters with the same title can have different compositions. The percentage of downregulated proteins that were found into significant clusters was 23, 29, and 47% for P, H, and PH conditions, respectively, and 37, 49, and 42% in the case of upregulated proteins. Small clusters (two to six proteins) were found among downregulated proteins. Most of these clusters were not specific to one condition and were retrieved totally or partly in at least two conditions (Table S4). For instance, protease-peptidase clusters (2–3 proteins) were found downregulated in P, H, and PH conditions. The largest downregulated cluster in P (four proteins) was related to chlorophyll biosynthesis and was also found in PH (Figure 9). The largest downregulated cluster in PH (six proteins) concerned proteolysis and was common to H and PH. Small clusters (3 proteins) connected to cell wall catabolism and photosynthesis (photosystem components and repair process) were also repressed in both H and PH. However, some small clusters were specifically downregulated in only one condition: rhodanese and peptidase in P; peroxidase in PH, and a larger one (translation, six ribosomal proteins) in H condition. This reflects a possible decrease of ribosomes in connexion with the inhibition of translation. The largest clusters (up to 17 proteins) were found for upregulated proteins (Figure 9; Table S4). The majority of the clusters upregulated in P were upregulated in PH as well but not in H, like the large protein folding cluster. In contrast, only a few chaperones were upregulated in H. Among them, interestingly, one of the HSP70 isoforms (HSP70-2) was specific only to the H condition. Small clusters related to sugar metabolism and TOPLESS corepressor were also common to P and PH. Most upregulated clusters shared by H and PH were connected to translation, signaling, proteasome, antioxidants (glutathione), protein import, pigment, and isoprenoid biosynthesis. The components of the upregulated translation cluster in H are different from those of the downregulated translation cluster associated with ribosomal proteins, which indicates

Figure 7. Impact of heat stress on the transcriptional profiles of genes involved in photosynthetic and respiratory electron transport chains.
Log2 ratio data for each treatment (P, H and PH) compared to control (C) were scaled from black to yellow for upregulated transcripts and from black to blue for downregulated transcripts. Heatmap was generated from http://bbc.botany.utoronto.ca/ntools/cgi-bin/ntools_heatmapper_plus.cgi. Genes were annotated according to Liang et al. (2016). The names of plastidial-encoded genes are colored in green and mitochondrial-encoded genes in orange.

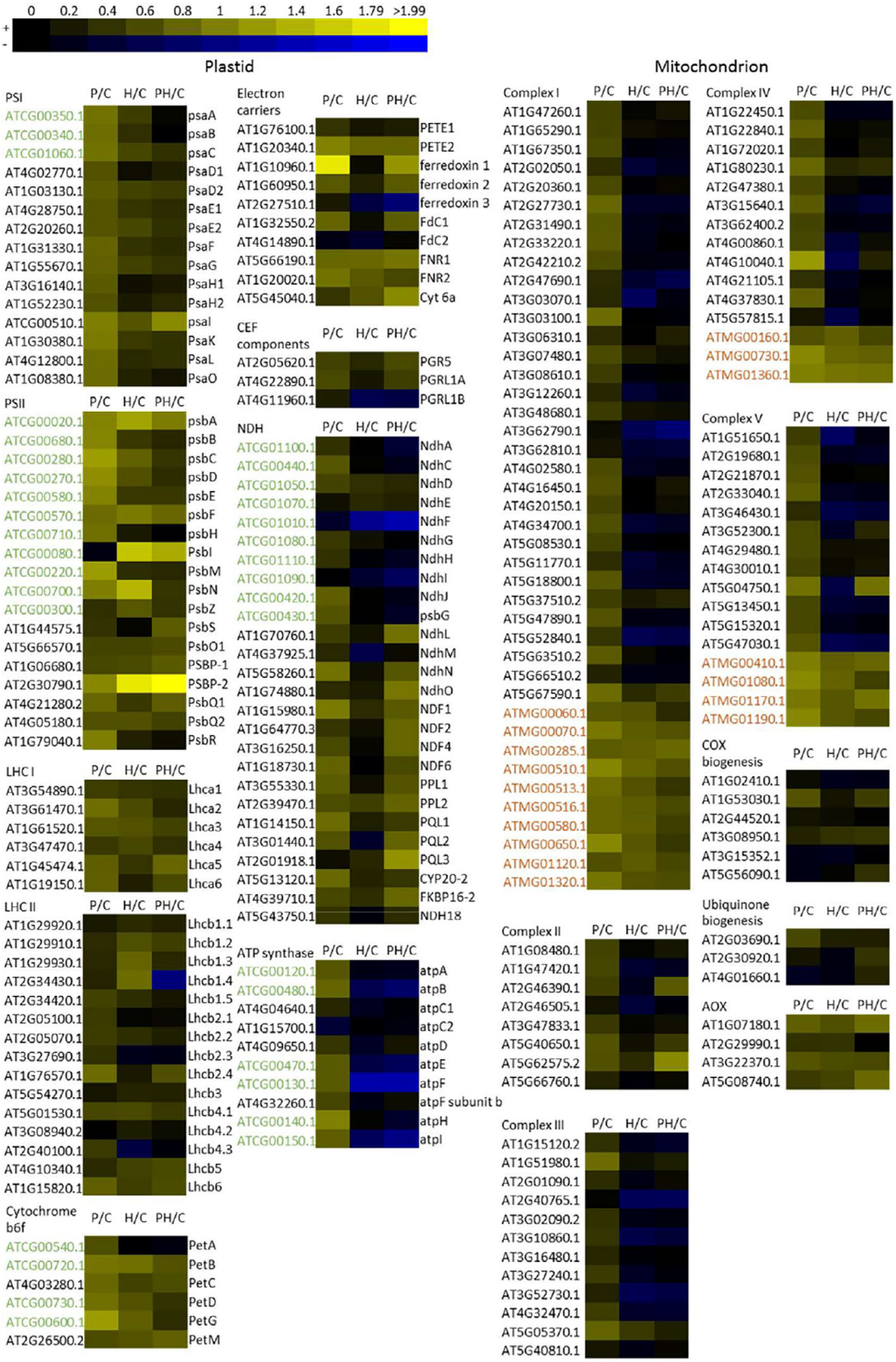

The Plant Journal, (2024), doi: 10.1111/tpj.16763

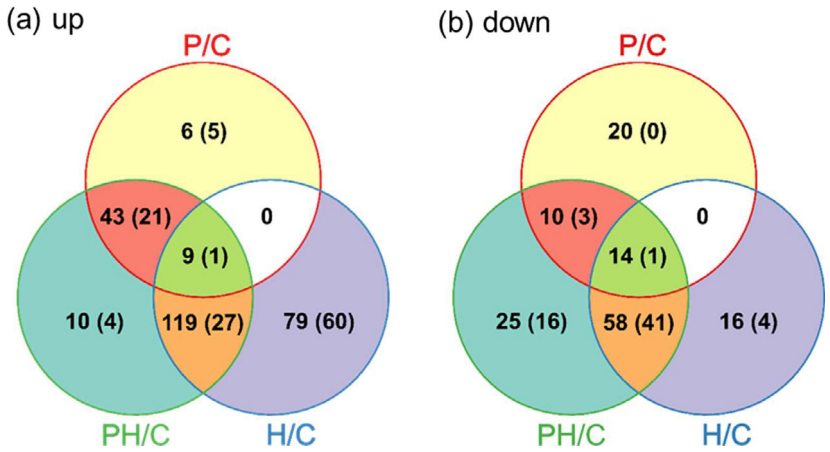

Figure 8. Responses of proteome to heat stress.
Venn diagrams representing the number of significantly accumulated (a) and decreased (b) proteins in response to the different heat stress regimes according to XIC quantification (ANOVA and Tukey test $P < 0.05$). The numbers between brackets correspond to the proteins showing variations with a ratio >2 or <0.5. Data were acquired before heat shock (P/C) or after 2 h of recovery post heat shock (H/C-and PH/C) without or with priming, respectively.

profound changes in the translation machinery triggered by heat shock. The analysis revealed that a major cluster (seven proteins) involved in protein import into the nucleus was present in H. This cluster was found partially in PH (two proteins) but not in P condition. Considering the importance of the HSR of nucleo-cytoplasmic exchanges, in particular through the shuttling of many transcription factors and co-activators required to modulate gene expression (Ohama et al., 2017), the reinforced expression of components of the nuclear import machinery under the heat shock makes sense. In the same way, a cluster of nine proteins connected to signaling and protein degradation was identified in H and only partly retrieved in PH but not in P condition. No cluster was specifically upregulated only in PH conditions. In contrast, several upregulated clusters (2–6 proteins) were found only in H. They were connected to carbohydrate and sulfur amino-acid metabolism, lignin biosynthesis, intracellular protein transport, protein dephosphorylation and degradation, and mitochondrial fission. Altogether, the STRING analysis has highlighted pathways that could be specifically upregulated upon priming (protein folding and chaperons, nucleotide sugar, TOPLESS) or heat shock (translation, protein import into the nucleus, antioxidants, isoprenoids). It was not surprising that these specific pathways were brought together in the PH condition, which mixed priming and heat shock.

Since the cluster analysis is essentially predictive and does not take into account the fold change and non-clustered proteins, we focused in more detail on the proteins displaying expression profiles that were common or specific to the different treatments. The shared response to all treatments included only nine accumulated proteins (Figure 8a), among which the first four were significantly upregulated at the transcriptional level in the different treatments: two HSP70 (AT3G12580.1; AT3G09440.1), Fes1A (AT3G09350.1), which was shown to contribute to thermotolerance by stabilizing cytosolic HSP70 (Zhang et al., 2010), a cyclophilin-like peptidyl-prolyl isomerase (AT1G01940.1), UGE1 (AT1G12780.1), involved in galactose synthesis, NINJA (AT4G28910.1) and TOPLESS-RELATED3 (AT5G27030) which are involved in the repression of the jasmonic acid signaling pathway (Pauwels et al., 2010), a peroxiredoxin (AT1G60740) and a chalcone flavanone isomerase (AT3G55120.1) called TT5. Among these proteins, only Fes1A showed a high fold change ratio ($\log2 > 2$) in all conditions, and HSP70 (AT3G12580.1) was the sole previously recognized as a member of the "common general heat stress response" in the study of (Echevarría-Zomeño et al., 2016). Differences in the experimental conditions and proteomics quantification methods likely explain such differences between studies. The 14 shared decreased proteins (Figure 8b) appeared involved in proteolysis (subtilase, AT2G05920.1; SPCL26, AT2G35780.1), defense (disease-resistance responsive proteins AT4G11210.1 and AT4G23690.1) or cell wall metabolism (ATEXLA1, AT3G45970.1; BXL1, AT5G49360.1; FUC95A, AT4G34260.1; SKS17, AT5G66920.1) (Table S3). Although most of these proteins are expected to be extracellular, according to SUBA4, we can make no clear link between their decreased abundance and heat stress.

Since PH seedlings can survive the otherwise lethal heat shock, we focused on the proteins significantly accumulating (ratio PH/C $\geq$ 2) under this condition (Table 1). In

Figure 9. STRING network analysis of the down/upregulated proteins in P, H and PH conditions.
Parameters used for STRING analysis are listed in Material and Methods. Cluster colors were assigned automatically by STRING. Only the principal clusters are shown and those containing more than three proteins are indicated by a keyword. The largest cluster is colored in red in each condition. Cluster lists and protein descriptions can be found in Supplementary information Table S3. Solid and dotted lines indicate connections within the same and different cluster, respectively. The line thickness indicates the strength of the data support. Clusters of two proteins and non-clustered proteins have been omitted from the figure. CWP = Cell wall polysaccharide; HSP = Heat shock protein.

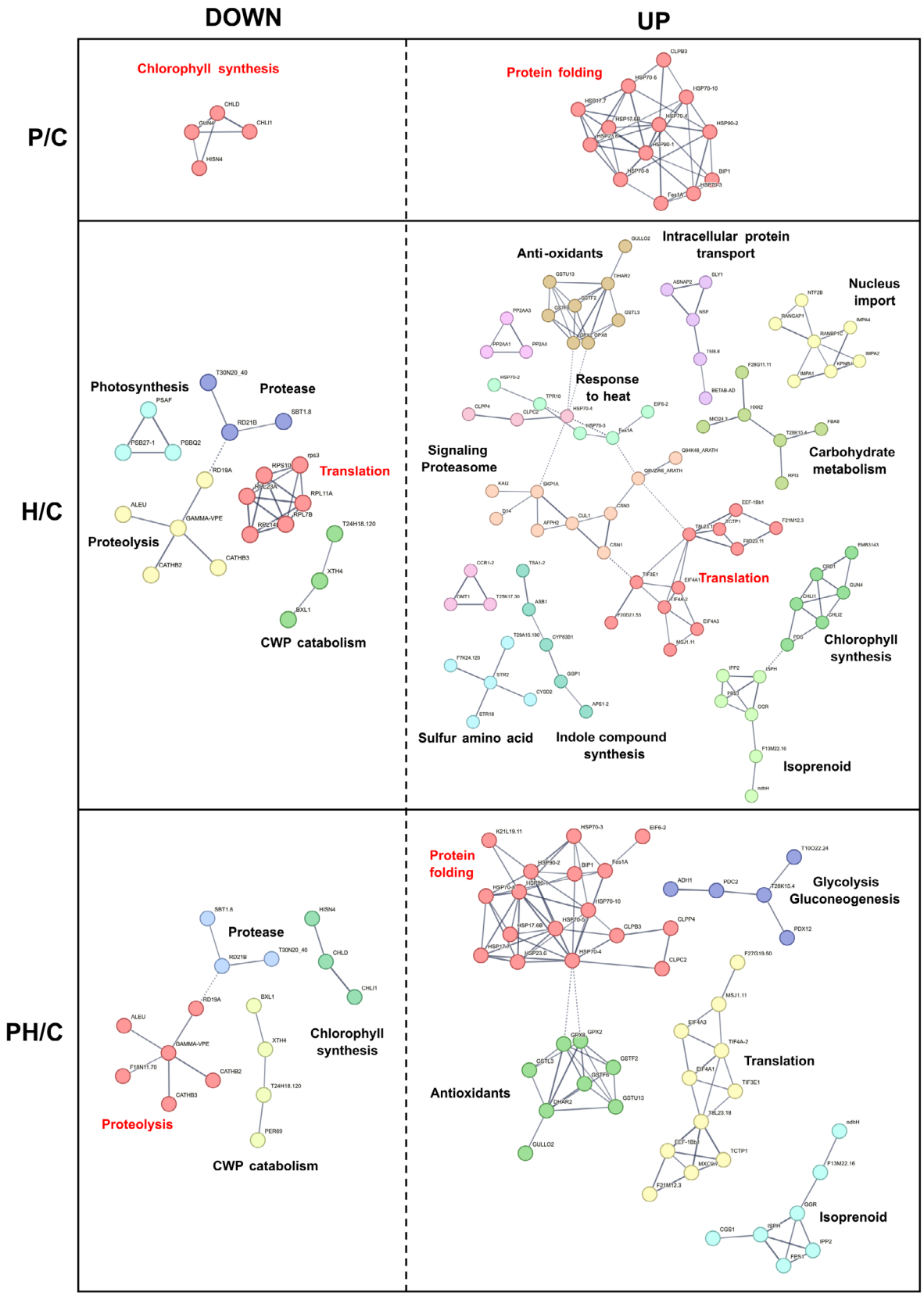

The Plant Journal, (2024), doi: 10.1111/tpj.16763

this list of 53 proteins, 13 proteins are related to protein folding or assembly, nine to signaling, six to chlorophyll and isoprenoid metabolism, 15 to various other functions, and ten proteins cannot be functionally classified beyond automatic annotation. The majority (28) was predicted to be cytosolic, eight plastidial, two mitochondrial, and seven nuclear, and the rest were assigned to various compartments (ER, Golgi, plasma membrane, vacuole). When examining the accumulation of these proteins in other conditions, only two proteins were found to accumulate exclusively in PH conditions: an uncharacterized chaperone binding protein (AT5G58110.1) and UBP1B (AT1G17370.1), which is involved in stress granule formation (Nguyen et al., 2016). Two complementary profiles emerged for the 51 other proteins, with 24 proteins accumulating also in P samples and 27 others accumulating in H samples. In most cases, the fold changes were similar between the PH and the other (P or H) conditions, which suggests that for these 51 proteins, their accumulation in PH samples reflects the effect of priming or heat shock. An exception is HSP17.6B (AT2G29500.1), whose expression is increased twice in the PH vs. P condition. Among the 15 proteins with the highest fold change (PH/C $\geq$4), 14 had already accumulated to a high level before heat shock, because of the priming treatment. They included several molecular chaperones such as three sHSP (HSP17.6A, HSP17.6B, HSP23.6), three HSP70 (HSP70T-2, HSP70, MTHSC70-2), HSP90-1, one HSP101 (CLPB3) and Fes1A which are co-chaperones of HSP70, but also the translation elongation factor EF1B and a putative peptidyl-prolyl cis-trans isomerase (AT1G01940.1). Except for HSP23.6 and MTHSC70-2, which are mitochondrial and CLPB3, which is plastidial, all these proteins are cytosolic. Another strongly over-accumulated protein in P and PH is pyridoxine biosynthesis 1.2 (PDX1.2), which was recently shown to play an essential role in maintaining vitamin B6 biosynthesis under heat shock (Dell'Aglio et al., 2017). According to a computational study, a protein (AT1G18270.1) displaying a 10-fold accumulation could play a role in ascorbate degradation (Zhang, Duan, et al., 2016), but how this would contribute to heat acclimation is not apparent. Among proteins involved in signaling and accumulating both in P and PH conditions, figures HKL, which is involved in heat signaling and memory (Sharma et al., 2019), the ER auxin binding protein ABP1 whose constitutive overexpression increased temperature sensitivity of hypocotyl growth (Gelová et al., 2021), and a poorly characterized transcription regulator (AT5G18230.1, NOT2/NOT3/NOT5 family protein). Noticeably, two proteins of unknown function display high accumulation levels in response to priming. AT3G10020.1 (PH/C = 16.8; P/C = 15) is annotated as a hypoxia unknown protein (HUP26), and AT1G30070.1 (PH/C = 5.0; P/C = 4.5) is annotated as an SGS domain-containing protein and was identified as a potential small ubiquitin-like modifier substrate (Elrouby & Coupland, 2010). This protein could intervene in the HSR since the SGS domain of another protein (SGT1) is responsible for HSC70 binding (Noël et al., 2007).

Among the proteins whose accumulation is triggered by the heat shock independently of priming (accumulating in H and PH conditions), seven chloroplast proteins were accumulating more than two-folds (Table 1). CGLD11 (AT2G21385.1) is involved in the assembly of the CF1 subcomplex of the ATP synthase (Zhang, Carter, et al., 2016). Another protein localized in plastoglobules (fibrillin FBN6) is expected to contribute to light acclimation (Lee et al., 2020). Four other accumulating proteins are involved in chlorophyll (NOL, CRD1) or isoprenoid metabolism (IPP2, HDR). The accumulation of these proteins in plastids under severe heat shock conditions reflects the need to counteract the damage to the photosynthetic apparatus. In the case of IPP2 (AT3G02780.1), it must be mentioned that although it is annotated as a chloroplast protein, there is strong evidence that its full-length isoform would be mitochondrial, while a shorter one would be peroxisomal (Phillips et al., 2008; Sapir-Mir et al., 2008). Curiously, another accumulated protein involved in isoprenoid metabolism (FPS1, farnesyl diphosphate synthase) is classified as cytosolic, but a long isoform was found to be mitochondrial (Closa et al., 2010; Cunillera et al., 1997). Collectively, our proteomic data suggest stimulation of the biosynthesis of isoprenoid precursors through the 2-C-methyl-D-erythritol 4-phosphate (MEP) pathway in the chloroplast (HDR) and through the mevalonate pathway (MEV) occurring in the cytosol, mitochondria (IPP2, FPS1) or even peroxisomes (IPP2). Several proteins accumulating in response to heat shock are involved in signaling pathways, like FUSCA6, a protein of the signalosome, CUL1, a component of auxin signaling or AT1G61150.1, a putative member of large eukaryotic signaling complexes of proteostasis (Tomaští ková et al., 2012), or the ER protein CYP83B1 which is involved in auxin biosynthesis (Maharjan et al., 2014). Finally, among proteins with diverse functions, an actin-depolymerizing factor (ADF2) accumulating in H and PH conditions could be related to the blockage of microfilaments and mitochondrial dynamics observed after treatment at 43°C.

The analysis of the 62 proteins with significantly reduced accumulation (ratio PH/C $\leq$0.5) in the PH condition revealed that 50 (80%) are similarly less abundant in the H condition. At the same time, most of them are not affected by priming (Table S3). This suggests that their decreased abundance is a direct consequence of heat shock. The list comprises 14 proteins annotated as proteases, seven proteins related to cell wall biogenesis and remodeling, two lipases, and an alpha-amylase. The decrease of proteins involved in catabolic processes could contribute to

Table 1 List of significantly accumulated proteins in PH seedlings ($P < 0.05$; PH/C ratio >2).

id	Description // Functional category	P/C	H/C	PH/C	loc
AT5G12030.1	AT-HSP17.6A // Molecular chaperone	18.91	0.82	18.76	c
AT3G10020.1	HUP26, Hypoxia response unknown protein 26 // Unknown function	14.96	1.18	16.86	n
AT3G09350.1	Fes1A // Protein folding	10.95	2.98	14.69	c
AT1G18270.1	Ketose-bisphosphate aldolase class-II family protein // Ascorbate degradation?	8.90	0.92	10.71	c
AT2G32120.1	HSP70T-2 // Molecular chaperone	10.03	1.13	10.16	c
AT2G29500.1	HSP17.6B // Molecular chaperone	4.13	1.14	8.66	c
AT4G25200.1	HSP23.6-MITO // Molecular chaperone	8.43	1.34	8.18	m
AT5G52640.1	HSP90.1 // Molecular chaperone	8.08	2.66	8.10	c
AT3G16050.1	PDX1.2 // pyridoxine biosynthesis	7.80	1.11	6.61	c
AT1G16030.1	Hsp70b // Molecular chaperone	4.52	1.29	5.65	c
AT2G21385.1	CGLD11, BFA3 // Protein assembly	1.29	5.19	5.26	pl
AT3G12580.1	HSP70 // Molecular chaperone	4.83	1.12	5.08	c
AT1G30070.1	SGS domain-containing protein // Unknown function	4.52	1.02	5.01	c
AT5G12110.1	Translation elongation factor EF1B/ribosomal protein S6 // Translation	4.30	1.64	4.70	c
AT1G66080.1	Hikeshi-like protein1, HKL, HLP1 // Heat signaling and thermomemory	4.16	1.73	4.26	c
AT5G47770.1	FPS1; farnesyl diphosphate synthase 1 // Isoprenoid metabolism	0.98	4.21	3.64	c/m
AT5G04900.1	NOL; NYC1-like // Chlorophyll metabolism	1.18	3.11	3.41	pl
AT3G03990.1	D14, DWARF 14 // Strigolactone signaling	1.46	2.42	3.18	c
AT1G61150.1	LisH and RanBPM domains containing protein // Signaling	1.28	5.10	2.97	n
AT5G19940.1	FBN6; Fibrillin 6 // Light stress acclimation	0.89	3.56	2.89	pl
AT3G56940.1	CRD1 // Chlorophyll metabolism	0.99	2.47	2.80	pl
AT5G15960.1	KIN1; stress-responsive protein // Unknown function	3.58	1.33	2.79	c
AT1G17370.1	UBP1B; oligouridylate binding protein 1B // Stress granule formation	1.72	1.36	2.79	n
AT5G18230.1	Transcription regulator NOT2/NOT3/NOT5 family protein // Transcription factor?	2.51	1.42	2.73	n
AT4G02570.1	CUL1, cullin 1; AXR6, auxin resistant 6 // Auxin signaling	1.38	3.29	2.68	n
AT5G15450.1	CLPB3; APG6 // Molecular chaperone	3.58	0.77	2.61	pl
AT2G45990.1	Ribosomal RNA small subunit methyltransferase G // Unknown function	0.73	3.66	2.58	pl
AT3G02780.1	IPP2 // Isoprenoid metabolism	0.68	3.19	2.56	pl/m/p
AT3G61140.1	FUSCA 6; COP9 Signalosome subunit 1 // Signalosome component	1.16	3.24	2.52	c/n
AT4G34920.1	PLC-like phosphodiesterases superfamily protein // Unknown function	0.95	2.86	2.41	c
AT4G31500.1	CYP83B1; SUPERROOT 2 // Auxin signaling	0.83	3.11	2.39	er
AT5G65020.1	ANNAT2; annexin 2 // Calcium signaling	1.04	2.84	2.31	c/pm
AT1G55450.1	S-adenosyl-L-methionine-dependent methyltransferases superfamily // Unknown function	0.83	2.92	2.29	g
AT5G58490.1	NAD(P)-binding Rossmann-fold superfamily protein // Unknown function	1.00	2.52	2.28	c
AT1G01940.1	Cyclophilin-like peptidyl-prolyl cis-trans isomerase family protein // Protein folding	2.00	1.59	2.27	c
AT1G13320.1	PP2AA3; protein phosphatase 2A subunit A3 //	0.83	3.97	2.27	c
AT4G34350.1	HDR; CLB6 // Isoprenoid metabolism	1.16	2.09	2.26	pl
AT1G71697.1	ATCK1, CK1; choline kinase 1 // Choline biosynthesis	0.87	2.19	2.25	c
AT1G60740.1	Thioredoxin superfamily protein PrxIID // Anti-oxidant	2.49	1.54	2.21	c
AT1G02930.1	ATGSTF6; glutathione S-transferase 6 // Redox metabolism	0.98	2.85	2.19	c
AT5G42080.1	ADL1, dynamin-like protein; RSW9, radial swelling 9 // Membrane organization	1.19	2.20	2.19	pm
AT3G42050.1	Vacuolar ATP synthase subunit H family protein // ATPase	0.87	2.46	2.18	v/g
AT5G58110.1	Chaperone binding; ATPase activators // Unknown function	1.07	1.72	2.16	n
AT5G20400.1	2-oxoglutarate and Fe(II)-dependent oxygenase superfamily // Flavone metabolism?	1.07	3.28	2.16	c
AT4G27450.1	HUP54, HYPOXIA RESPONSE UNKNOWN PROTEIN 54 // Unknown function	2.28	1.06	2.15	c
AT4G02980.1	ABP1; auxin binding protein 1 // Auxin signaling	2.04	1.44	2.12	er
AT1G68300.1	Adenine nucleotide alpha hydrolases-like superfamily protein // Stress response?	2.40	1.35	2.11	pm
AT5G43450.1	2-oxoglutarate and Fe(II)-dependent oxygenase superfamily protein // Ethylene metabolism?	1.05	2.18	2.10	c
AT5G09590.1	HSC70-5; mitochondrial HSO70 2 // Molecular chaperone	1.96	1.18	2.08	m
AT5G19820.1	EMB2734, embryo defective 2734; KETCH1 // Micro RNA processing	0.97	2.97	2.05	g
AT3G07090.1	PPPDE putative thiol peptidase family protein // Unknown function	2.37	0.98	2.02	c
AT3G46000.1	ADF2; Actin depolymerizing factor 2 // Microfilament dynamics	0.70	2.86	2.01	c
AT3G29350.1	AHP2; histidine-containing phosphotransmitter 2 // Cytokinin signaling	0.88	2.42	2.01	c

Proteins whose ratio are highlighted in red are significantly accumulated, and in green decreased, in the treatment compared to the control condition. Green background denotes proteins with specific accumulation in P and PH samples and yellow background proteins with specific accumulation in H and PH samples. Loc: location according to SUBA4con; c: cytosol; er: endoplasmic reticulum; g: Golgi; m: mitochondrion; n: nucleus; p, peroxisome; pl: plastid; pm: plasma membrane; v: vacuole. Alternative localisations have been indicated for AT5G47770.1, AT3G02780.1, AT3G61140.1, AT5G65020.1 and AT3G42050.1.

maintaining proteostasis and reinforcing cell walls in conditions where translation is blocked. Most of these proteins are cytosolic or extra-cellular. Still, eight are expected to be plastidial, including two PSII subunits (PSBQ, PSBP) and CCD4, which are involved in carotenoid degradation in seeds and senescing leaves (Gonzalez-Jorge et al., 2013).

While many protective proteins like HSPs accumulated in PH and P conditions, 79 proteins were found to specifically accumulate in the H condition (Table S3). They included components of "ubiquitin-dependent protein catabolic process" GO (ubiquitin C-terminal hydrolase 3 (UCH3), S phase kinase-associated protein 1 (SKP1), regulatory particle non-ATPase 13 (RPN13), ubiquitin-conjugating enzyme 35 (UBC35), constitutive photomorphogenic 13 (COP13), UBC36 (ubiquitin-conjugating enzyme 36)) and of "protein transport" (Arabidopsis RAB GTPase homolog A2C (ATRAB-A2C), homolog of human KPNB1, translocase of the inner mitochondrial membrane 13 (TIM13), alpha-soluble NSF attachment protein 2 (ALPHA-SNAP2), ATSLY1, Adaptin family protein, RAN binding protein 1 (RANBP1), importin alpha isoform 2 (IMPA2)). Moreover, a set of 16 proteins was found to be specifically downregulated in the H condition, including six ribosomal proteins (RPL7B, RPL16A, RPL14 family protein, RPL14p, RNA binding plectin/S10 domain-containing protein and chloroplast ribosomal protein S3) and two proteins involved in poly(A) mRNA export and splicing MOS11 (modifier of SNC1) and SCL30 (SC35-like splicing factor 30). Collectively, these data favor a strong disturbance in protein synthesis and degradation under H conditions compared to PH, even after 2 h of recovery post-heat shock.

We also performed a sPLS–DA analysis on the whole set of proteins whose abundance was quantified by XIC analysis. The analysis identified two components that discriminate heat shock and priming samples, respectively (Figure S5). The full list of discriminative variables selected for component one (10 proteins) and component two (60 proteins) is indicated in Table S5. The first component explained 32.6% of variance in protein level and discriminate proteins that were highly upregulated in H and to a lesser extend in PH compared to the control. The second component explained 13.3% of the variance in protein level and mostly discriminate proteins that were highly upregulated in P and PH compared to control. No gene ontology was found for the ten proteins selected on the first component. However, the first protein was a glutathione S-transferase (AT1G02930.1), which is possibly related to oxidative stress. The proteins selected on the second component were associated with stress response and protein folding by Gene Ontology (Figure S5). Among these 60 proteins, 18 are chaperones or related proteins (Table S5), which confirmed their importance for heat acclimation and heat shock tolerance. HUP26, a hypoxia response unknown protein (AT3G10020), which was highly upregulated in P and PH, was found to be the most discriminative variable.

Time-course of HSP accumulation

Since chaperones are major thermotolerance components, we looked closer at the evolution of their abundance after the different treatments. The XIC results of the shotgun proteomic analysis revealed that, apart from a few that did not accumulate after heat stress (CPLC, Hsc70-1, BDS2), most were highly increased in P and PH conditions, but not in the H condition, like several cytosolic HSPs (HSP90.1, HSP70B, HSP70T-2, HSP70, HSP17.6, HSP20-like) and the mitochondrial HSP23.6 (Figure S6a). This was also confirmed for several other HSPs that could not be quantified using XIC but were readily detected by spectral counting method in both P and PH samples but not in C and H samples, such as the plastidial HSP21, the mitochondrial HSP26.5 and HSP23.5 or the cytosolic HSP101 (Figure S6b). We used a complementary approach of immunodetection to visualize the abundance of several HSPs (HSP101, HSP70, plastidial HSP70, HSP17.6, plastidial HSP21 and mitochondrial HSP26.5) during priming, heat shock and recovery period (Figure 10; Figure S7). HSP101 was rapidly accumulated in the P condition (after 30 min of treatment) and maintained after priming. The protein was not detected in the H sample, whereas its level remained stable before, during, and after heat shock in PH samples. The cytosolic and chloroplastic HSP70 increased slightly after priming but remained stable in H and PH conditions. It is noteworthy that, since the anti-cytosolic HSP70 antibody is susceptible to detect three constitutive (HSC70-1, HSC70-2, HSC70-3) and two heat-inducible cytosolic HSP70 (HSP70-4, HSP70-5), it is not possible to correlate the immunoblot results with variations of these HSP isoforms detected with proteomics. In the case of chloroplastic HSP70, the antibody is expected to recognize both cpHSC70-1 and cpHSC70-2, but these isoforms were not detected in our proteomic analysis. A more detailed investigation of HSP70 response would require specific antibodies. The small HSPs (HSP21, HSP17.6, HSP26.5) were detected in P samples from 2 h of treatment, and their level increased during recovery (Figure 10; Figure S7). They were, however, undetectable in H samples at any time of stress or recovery. In the PH condition, these proteins, which were present before the stress because of the priming, almost disappeared during the treatment, to reappear progressively during the recovery period. We hypothesized that these proteins were not soluble anymore at 43°C because of co-aggregation with other proteins, as shown for the pea HSP22 (Avelange-Macherel et al., 2020). We, therefore, separated the supernatant and pellet after tissue lysis (Figure 10b). Interestingly, a large proportion of HSP17.6 and HSP21 could be detected in the pellets, especially in PH condition, which supports the hypothesis of

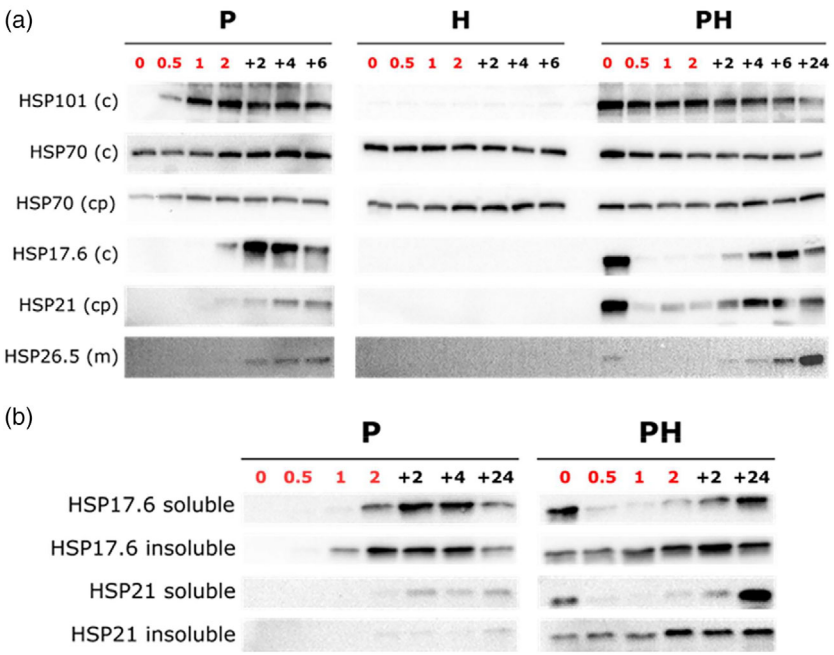

Figure 10. HSP profiles in response to heat shock.
(a) Representative immunoblots of HSPs in response to the different heat treatments. Numbers denote the number of hours of heat stress (in red) or recovery period (black).
(b) Representative immunoblots of HSPs present in the soluble protein extract (soluble) and in tissue pellet (insoluble) in response to the different heat treatments. Numbers denote the number of hours of heat stress (in red) or recovery period (in black).

co-precipitation of these sHSP with client proteins during heat shock (Waters, 2013; Waters & Vierling, 2020). Such a mechanism could facilitate the work of disaggregases, and both cytosolic sHSPs and HSP101 contributed to the protection of translation elongation factors during heat stress (McLoughlin et al., 2016). Moreover, HSP101 was previously shown to be involved in the release of ribosomal proteins mRNA during the recovery period (Merret et al., 2017), which would also contribute to a faster recovery of translation in PH seedlings, compared to H seedlings. The accumulation of HSP101 protein was also correlated with seedling survival to heat shock in different ecotypes of Arabidopsis (Zhang et al., 2015). Hence, the accumulation of HSP101 and sHSPs observed upon priming, together with the likely co-precipitation of sHSP during the subsequent heat shock, suggests a role in the protection of the translational machinery that cannot be fulfilled in the case of the noxious H condition. Overall, these results confirmed the necessity of several HSP accumulation and persistence in various cellular compartments for acquiring thermotolerance, but also how critical is the preservation of the translational apparatus.

Correlation between transcriptomic and proteomic data

Integration of transcriptomic and proteomics data allowed us to examine the overall relationship between the variations in the abundance of proteins (according to XIC) measured after recovery and their transcript level variation after 30 min of stress. The determination of Pearson's coefficient revealed moderate positive correlations between protein and transcript levels for both P and PH conditions (r = 0.71 and 0.64, respectively). In contrast, there was no statistically significant correlation in the case of the H condition (Table 2). Among the 58 proteins significantly accumulated in P (after 22 h of recovery), 32 (55%) of their transcripts were also significantly overexpressed after 30 min of heat treatment, whereas only 4 out of 44 (9%) proteins with decreased abundance were also downregulated at the transcriptional level (Table 2). In H seedlings, 207 proteins accumulated, among which only five (2.4%) had their transcripts upregulated, while only seven out of 88 (8%) proteins with decreased amounts had their transcripts downregulated. In PH seedlings, 181 proteins accumulated, among which 33 (18%) were also upregulated at the transcriptional level. For the 107 proteins with decreased amounts, 26 (24%) had their transcripts downregulated. Interestingly, the highest correlation was for the increased proteins in P samples, even though the transcriptomic and proteomic data were acquired with a one-day lag, compared to less than 4 h for H or PH samples. This is likely because most of the proteins accumulating after priming remain present 24 h later. However, a detailed kinetics of transcriptomic and proteomic changes occurring during and after heat

Table 2 Correlation between changes in protein and transcript abundance.

Protein	Transcript	P/C	H/C	PH/C
+	+	55.2% (32/58)	2.4% (5/207)	18.2% (33/181)
+	−	0% (0/58)	1.0% (2/207)	1.1% (2/181)
+	0	44.8% (26/58)	96.6% (200/207)	80.7% (146/181)
−	−	9.1% (4/44)	8.0% (7/88)	24.3% (26/107)
−	+	0% (0/44)	2.3% (2/88)	5.6% (6/107)
−	0	90.9% (40/44)	89.8% (79/88)	70.1% (75/107)
Pearson		0.71	0.10	0.64
P-value		3.0 E-58	0.06	4.4 E-44

For each treatment, proteins significantly accumulated (+) or decreased (−) (according to XIC quantification, $P < 0.05$) were classified depending on whether their transcripts were significantly overexpressed (+), downregulated (−) (FDR <0.05, log2 ratio >1 or <−1) or not significantly affected (0). Both the proportion and the fraction of proteins (between brackets) in each class are indicated.

treatment would be necessary to provide a more comprehensive view of transcriptional and translational regulation upon priming and heat shock. Nevertheless, the data agree with the severe impact of heat shock on translation, as reflected by the low correlation between the transcripts and protein levels in H, whereas PH is in between the P and H conditions (Table 2). Although we did not measure its activity, our data suggest that translation was severely impaired under heat shock, which agrees with previous work (Yángüez et al., 2013). Therefore, the relatively large set of 207 proteins detected with a higher abundance than in the control after 2 h of recovery were necessarily synthesized after the heat shock. Since the correlation with their transcript levels during early stress exposure is very low, how can we explain their accumulation? If we consider a transcriptional regulation, these proteins were likely to be translated using transcripts having accumulated during later heat shock exposure or/and early stress recovery. However, this view remains naive, not only because of the complexity of translational control (Shoemaker & Green, 2012) but also because the impairment of translation occurring under heat shock has a substantial impact on RNA quality control by triggering a massive decay of translating mRNAs (Merret et al., 2015). A more detailed kinetic analysis of the transcriptome during and after HS would be of interest to dissect the mechanisms governing the accumulation (or decrease) of proteins highlighted in our study.

Heat shock-induced metabolic disturbance is rapidly recovered in primed seedlings

Considering the importance of primary metabolism in plant growth and stress tolerance, we performed targeted metabolic profiling of amino acids, organic acids, and sugars after priming, just after heat shock, and during the recovery period (Figure 11; Table S6). Clustering analysis indicated that primed seedlings' metabolic profile was similar to that of control seedlings (Figure 10a). The main differences were a significant increase in the concentration of malate (1.2×), fructose (1.9×), and raffinose (10×) and a decrease in the concentration of oxo-glutarate (0.7×). In contrast, all amino acid concentrations were not significantly affected by the treatment (Table S3). The global metabolic profile of PH seedlings just after heat shock and after 2 h of recovery was nearer to that of H seedlings than to those of P or control seedlings (Figure 10a). Except for Asn, Cys, Glu, Gly, and Ser concentrations that remained unchanged, amino acid levels increased on average by 3-fold after heat shock in H and PH seedlings compared to the control condition (Table S6). The highest increase was observed for Arg (5.6×) and Pro (4.5×). The overall amino acid amount was very similar in H and PH seedlings just after heat shock. After 2 h of recovery, Asp continued to accumulate significantly while Ala amount decreased in both H and PH seedlings (Table S6). The fact that there was no significant difference in the accumulation of most amino acids between H and PH, even after 2 h of recovery post-heat shock, suggests that amino acid metabolism is not a significant component of the protective effect of priming. The rise in the pool of branched-chain, aromatic, and also of oxoglutarate-derived amino acids (Pro and Arg) is in agreement with previous work (Caldana et al., 2011; Kaplan et al., 2004), although the temperature applied was higher in our study (43°C) than in the others (40 and 32°C, respectively). Branched-chain amino acids may act as compatible solutes or provide an alternate electron donor to the mitochondrial electron transport chain (Obata & Fernie, 2012), while accumulation of aromatic amino acids could be related to auxin or glucosinolate metabolism as precursors (Tzin & Galili, 2010). However, the increase in Pro observed in both H and PH seedlings contradicts another work, which showed that acclimation led to a lower rise in Pro level, in agreement with the toxicity of Pro under high temperatures (Larkindale & Vierling, 2007). Another study showed that Pro over-accumulation under heat stress led to an increased generation of ROS and decreased ethylene and ABA synthesis (Lv et al., 2011). Osmolytes like proline have indeed be shown to

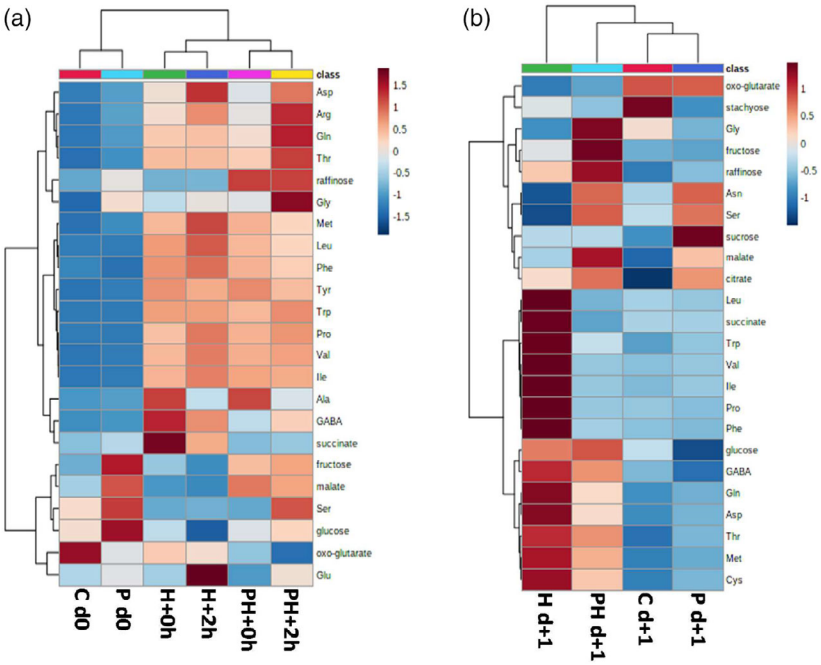

Figure 11. Responses of primary metabolism to heat stress.
(a) Heatmap clustering analysis representing the changes in abundance of sugars, organic and amino acids in seedlings before heat shock (C: control; P: priming), just after heat shock (H: heat-shock; PH: priming + heat shock) and 2 h after heat shock (H+2 h; PH+2 h).
(b) Heatmap clustering analysis representing the changes in abundance of sugars, organic and amino acids in seedlings 24 h after heat shock application. The metabolites shown on the heatmaps were significantly differentially affected by at least one condition according to ANOVA ($P < 0.05$). Analysis was performed using MetaboAnalyst 4.0 with the Euclidian distance method and ward clustering algorithm after Pareto scaling.

favor protein stability and chaperone activity but also to increase protein aggregation at high concentration (Diamant et al., 2001), which could explain such discrepancies. In our conditions, the accumulation of Pro was not correlated with survival or later death of seedlings since it accumulated to a similar extent in H and PH.

After heat shock, there was no variation in the amounts of glucose or fructose, and therefore the fructose level that had increased upon priming remained higher in PH seedlings. The oxoglutarate concentration lowered by priming was also lower than in control for H and PH seedlings (0.7 and 0.4×, respectively) after 2 h of recovery. Several metabolites were nevertheless differentially impacted in PH and H seedlings just after heat shock or after 2 h recovery (Figure 11a). In PH seedlings, the level of raffinose was significantly higher than in P seedlings (2.4×) and C seedlings (24×), whereas it did not increase significantly in H seedlings compared to the control condition. This agrees with the work of (Serrano et al., 2019), who found that the accumulation of raffinose family oligosaccharides was a major response to priming. In the context of the HSR, these compounds could play the role of chemical chaperones, as demonstrated *in vitro* for the related di-saccharide trehalose (Diamant et al., 2001). In contrast, GABA concentration increased by 2-fold in H seedlings after heat shock compared to control but remained unchanged in PH seedlings compared to C and P seedlings. In addition, Leu, Met, and Glu further accumulated after 2 h of recovery in H seedlings but not in PH seedlings (Table S6). We further investigated the metabolic response after 24 h of recovery, which revealed more drastic changes (Figure 11b, Table S6). After a longer-term recovery, the global metabolic profiles of H and PH seedlings differed significantly, and clustering analysis showed that the PH seedling profile was closer to P seedling (Figure 11b). The abundance of several amino acids (Asp, Cys, Gln, Ile, Leu, Met, Phe, Pro, Thr, Trp, and Val) and GABA remained significantly higher in the H condition compared to the control condition (Table S6). However, in PH seedlings, the concentration of Ile, Leu, Phe, Pro, and Val decreased back to control values, and that of Asp, Cys, Gln, Thr, and Trp was in between control and H levels.

We further examined whether metabolite variations in H and PH seedlings, compared to the control condition, could be correlated with changes at the transcript and protein level (transcripts at 30 min of stress, proteins and metabolites after 2 h of recovery). Although such an analysis is limited by data availability, we could provide reasonable evidence for a coordinated response for plastidial branched-chain and aromatic amino acids, which accumulate following heat shock (Figure 12). The genes involved in the biosynthesis of Ile, Val, and Leu, *AHASS1* (acetolactate synthase small subunit 1), *BCAT-2* (branched-chain-amino-acid aminotransferase 2), and *IPMI2* (isopropylmalate isomerase 2) were overexpressed in both H and PH conditions, whereas *IMD2* (isopropylmalate dehydrogenase 2) was only overexpressed in PH seedlings (Figure 12b). However, at the protein level, a significant accumulation was only detec ted for IPMS1 (isopropylmalate synthase 1) in PH samples after 2 h of recovery. In Tyr and Trp biosynthetic pathways, several genes were also significantly upregulated: *SK1* (shikimate kinase 1) in PH seedlings; *TyrAAT2* (arogenate

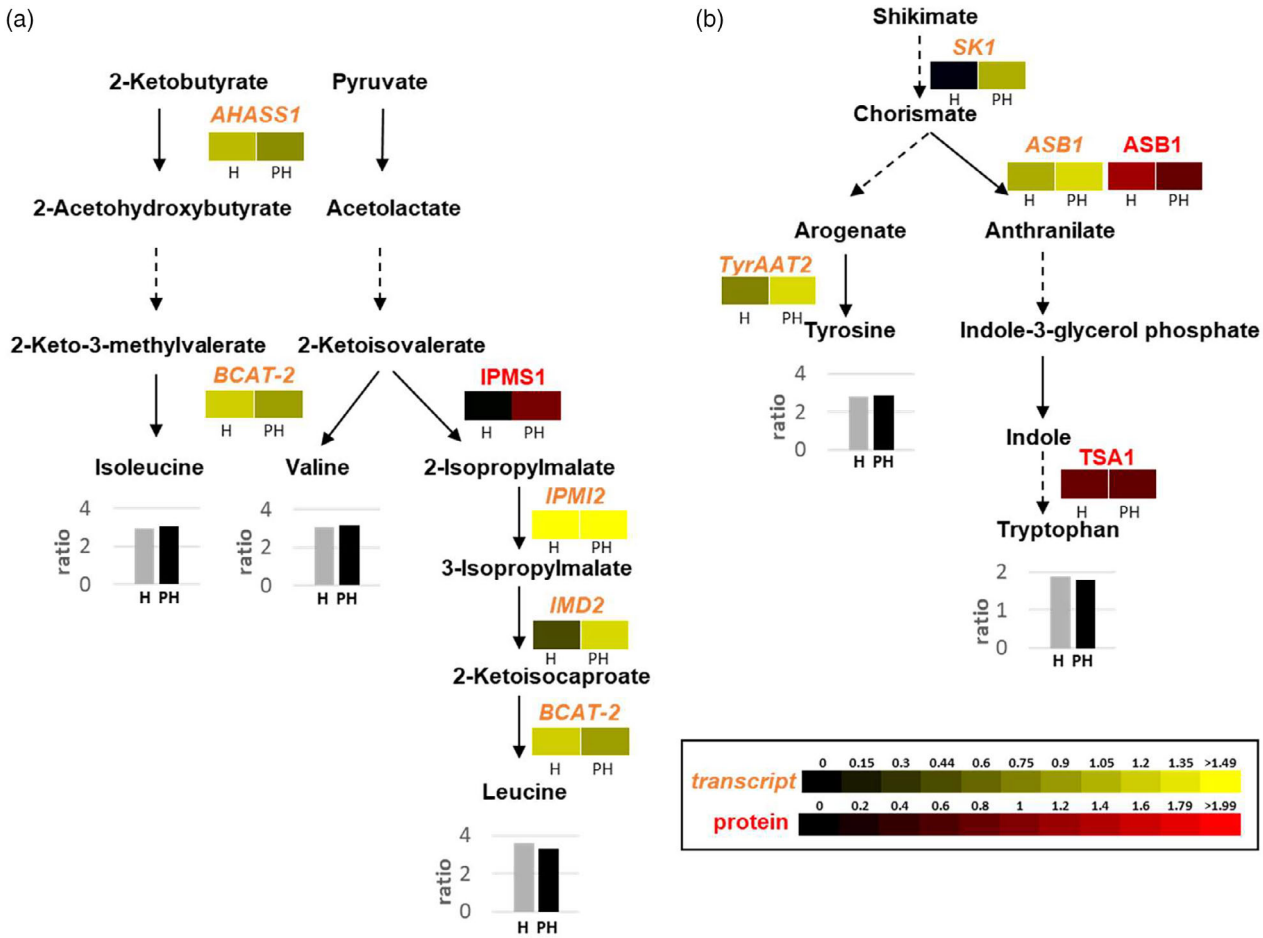

Figure 12. Transcriptional, proteomic and metabolic responses of branched chain and aromatic amino acids pathways in the plastids under heat shock. Plastidial biosynthetic pathways of Ile, Val and Leu (a) and Trp and Tyr (b) are shown, together with enzymes that were significantly upregulated at the transcript and/or protein level after heat shock ($P < 0.05$). Transcripts were analyzed after 30 min of heat shock at 43°C and proteins and metabolites after 2 h of recovery. Transcripts are indicated in italics. The green and red heatmaps correspond to the log2 ratio of H/C and PH/C at the transcript and protein level, respectively. Bar graphs show metabolite concentration ratio of H/C (gray) and PH/C (black). AHASS1, ACETOLACTATE SYNTHASE SMALL SUBUNIT 1; ASB1, ANTHRANILATE SYNTHASE BETA SUBUNIT 1; BCAT-2, BRANCHED-CHAIN AMINO ACID TRANSAMINASE 2; IMD2, ISOPROPYLMALATE DEHYDROGENASE 2; IPMI2, ISOPROPYLMALATE ISOMERASE 2; IPMS1, ISOPROPYLMALATE SYNTHASE 1; SK1, SHIKIMATE KINASE 1; TSA1, TRYPTOPHAN SYNTHASE ALPHA CHAIN, TyrAAT2, AROGENATE DEHYDROGENASE 2.

Dehydrogenase2) and *ASB1* (anthranilate synthase beta subunit) in both H and PH conditions. At the protein level, ASB1 and TSA1 accumulated more in H seedlings than in PH seedlings after 2 h of recovery. For the genes mentioned above involved in branched or aromatic amino acid biosynthesis, transcripts and proteins increased on average by 2-fold compared to control except for *IPMI2* (8- to 9-fold). The upregulation of several plastidial enzymes, either at the transcriptional or at the protein level, was well correlated with the increase in aromatic and branched-chain amino ac ids during heat shock, suggesting that this accumulation resulted from an increased biosynthetic capacity in plastids.

Looking at the other pathways, in both H and PH seedlings, Gln accumulation (2.7 and 3.8×, respectively) could be correlated with the upregulation of *ASE3* (Gln phosphoribosyl pyrophosphate amidotransferase) (log2 fold change of 1.3 and 1.5, respectively, Table S1). In PH samples, the *P5CS1* gene (Δ-1-pyrroline-5-carboxylate synthetase 1) of proline biosynthesis was repressed (log2 fold change −1.5). In contrast, the *ProDH* and *P5CDH* genes (proline dehydrogenase and Δ-1-pyrroline-5-carboxylate dehydrogenase) in proline catabolism were over-expressed (log2 fold change of 1 and 1.4, respectively), but this does not correlate with Pro accumulation observed in both H and PH seedlings (5.4 and 5×, respectively). Although the increase of Arg in H and PH seedlings was impressive (8.3 and 10.5×, respectively after 2 h of recovery), no change in the transcripts or proteins involved in Arg biosynthesis was observed. Therefore, this increase could result from metabolic regulation or a decrease in Arg catabolism. Arg is a precursor of polyamines (Bitrián et al., 2012), which were shown to accumulate during heat stress in wheat

(Goyal & Asthir, 2009). Interestingly, arginine decarboxylase 1, an enzyme involved in the synthesis of putrescine from Arg, is significantly downregulated at the transcriptional level in P, but in H and PH, the log fold change is lower (−1.15, −0.78, and −0.75, respectively).

Regarding sugar metabolism, galactinol synthase is an enzyme involved in raffinose and galactinol synthesis previously identified as an HSF target (Panikulangara et al., 2004). It was significantly upregulated at the transcriptional level in P and PH seedlings (log2 fold change 6.9 and 6.2, respectively). Moreover, UGE1, an enzyme involved in galactose synthesis, a precursor for galactinol and raffinose biosynthesis, was also upregulated in both treatments at the protein level (1.4× in P and 1.9× in PH). These results fit with the 10× fold and 24× fold raffinose accumulation observed in P and PH seedlings. However, in H seedling, galactinol synthase transcript and UGE1 enzyme were also overexpressed (log2 fold change of 2.26 and fold change of 2.3, respectively), but without raffinose increase. It is, therefore, difficult to assume that the accumulation of raffinose would only rely on the induction of its biosynthetic pathway.

On the whole, it appears that the accumulation of a few metabolites in PH and/or H conditions can be related to an increase in transcripts and proteins of their biosynthetic pathways. For other metabolites, a more comprehensive analysis would be needed to explain their dynamics, including the transcriptional and proteomic responses for enzymes involved in primary metabolism after 24 h of recovery.

DISCUSSION

Because of global warming, plants and crops in many regions worldwide are increasingly exposed to heatwaves whose duration and severity compromise their survival, with dramatic consequences for the ecosystems and crop production that we now directly observe. Understanding how plants can react and eventually tolerate extreme heat is primordial in this context. Although much is known about the general response (e.g., the ubiquitous HSR) and the importance of priming, there are still many gaps to fill, particularly by addressing critical issues such as the tissue temperature, the developmental stage, and the recovery period (Jagadish et al., 2021). In most studies carried out with plants in natural or controlled environments (either in soil or in solid media), the actual temperature of the plant tissues, which can significantly differ from the air temperature and be highly variable, is unknown. This is not the case in our model system, where seedlings are continuously maintained in water and thus precisely at the imposed temperature. Although the growth conditions are very different from those faced in a natural environment, we have previously shown that such seedlings remain fully viable for weeks since they resumed normal development when transferred to soil (Réthoré et al., 2019). Since the seedlings are autotrophic but arrested in their development because of mineral nutrient starvation, their metabolism was shown to be primarily devoted to photosynthesis, respiration, and photorespiration to dissipate light energy while maintaining homeostasis. The fact that these seedlings can acquire thermotolerance after a short priming treatment demonstrates that they display typical plant stress and acclimation responses, as reported for various crops and model species (Liu et al., 2021). Thus, our experimental model allowed us to address the effect of priming on heat shock tolerance at different scales, including physiological, cell biology, transcriptomic, proteomic, and metabolic responses, with the main results being schematized in Figure 13, with emphasis on energy-transducing organelles.

Protection of respiration and photosynthesis

A significant effect of priming was attenuating the substantial and irreversible inhibition of respiration and photosynthesis during heat shock, followed by the complete restoration of these processes within 24 h of recovery. Hence, photosynthesis and respiration under heat shock and initial recovery are robust predictors for later survival or death and thus major determinants for tolerance to toxic heat stress. We found that respiration was much more strongly affected than photosynthesis by the 43°C treatment, although photosynthesis is generally expected to be more thermolabile (Posch et al., 2019; Scafaro et al., 2021). This apparent discrepancy likely results from the fact that it is challenging to compare long-term exposure to increasing temperature with heat shock treatments, for which simultaneous measurements of photosynthesis and respiration have not been reported before, to our knowledge. However, the priming treatment performed the day before the noxious heat shock promoted acclimation of photosynthesis and respiration like it would occur for plants exposed to recurrent heat waves (Scafaro et al., 2021). Protection of energy transduction capacity should be primordial for plants exposed to severe stress, such as the 43°C heat shock used in this work, because a shortage of ATP would hamper the function of HSR actors such as the molecular chaperones, and large amounts of ATP would be needed to fuel the resumption of translation upon stress relief. Indeed, although plants adapt themselves during stress by reducing energy consumption through selective mRNA translation (Branco-Price et al., 2008; Yángüez et al., 2013), it is clear that recovery of translation processes would require much energy, in the order of three ATPs per new peptide bound to be formed, once ribosomal protein mRNAs are freed from stress granules with the help of HSP101 proteins (Merret et al., 2017). At the protein level, more than 50 plastidial and a dozen mitochondrial proteins were found to accumulate following the heat

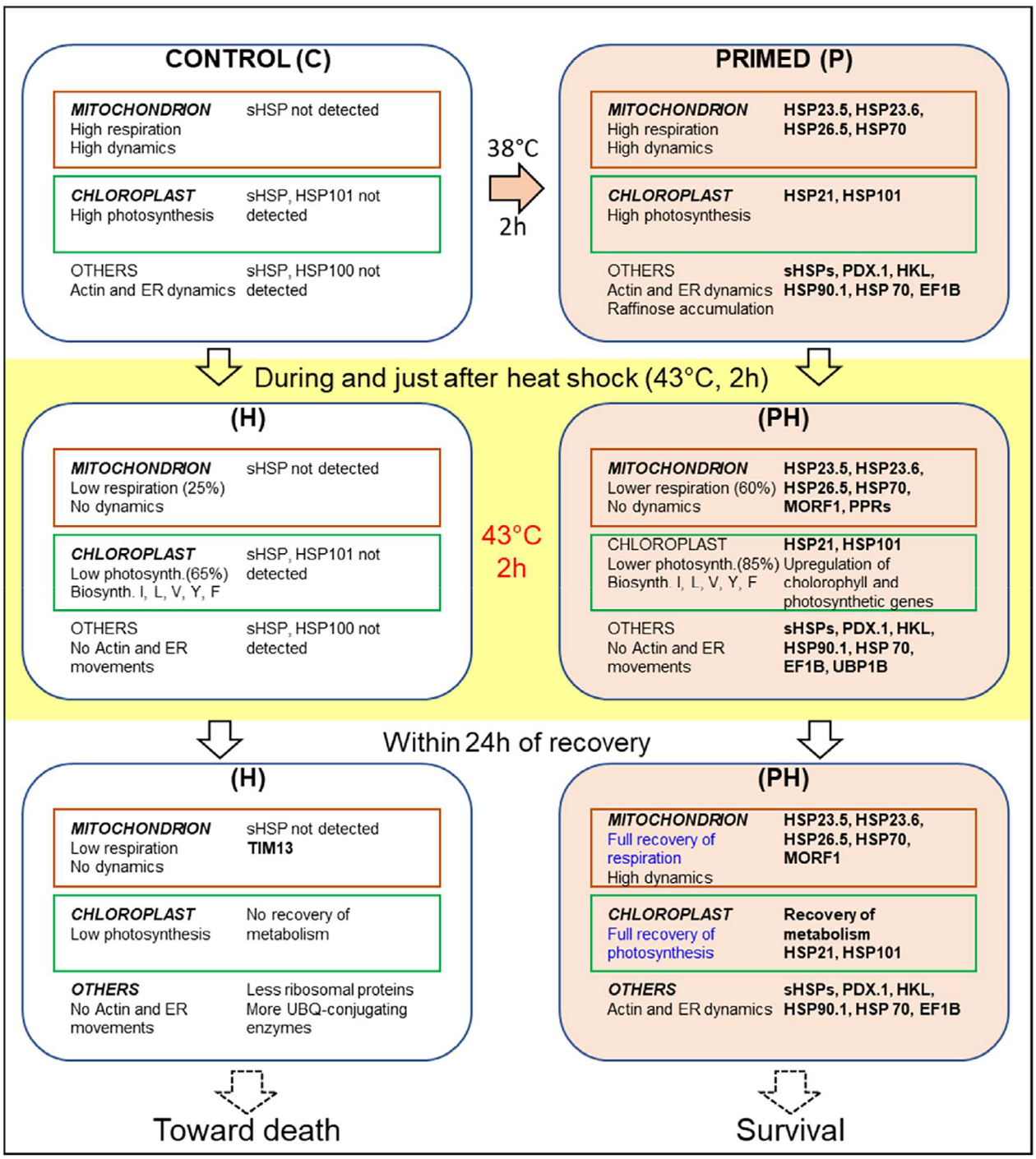

Figure 13. Overall response to heat-shock of mitochondrion, chloroplast and other compartments.
The scheme highlights the main components of the cellular responses of seedlings to temperature identified in this study. Primed seedlings have normal energy metabolism and organelle dynamics but have accumulated inducible HSPs in organelles and cytoplasm. When the primed seedlings are exposed to the noxious heat shock, their photosynthetic and respiratory functions are less affected than in the case of control seedlings, and they still maintain biogenesis. After 24 h of recovery, the activity of mitochondrion and chloroplast are fully recovered in the primed seedlings, allowing seedling survival, whereas the low metabolic activity in the unprimed seedlings leads to death.

shock (H and PH conditions). Apart from a signature about chlorophyll and isoprenoid metabolism, and hence a likely link with the maintenance of photosynthetic antennae, there is no major evidence besides chaperone accumulation for specific protection of these organelles. However, we cannot rule out that slower modifications occur

because a single time point was analyzed (2 h after heat shock).

Mitochondrial dynamics

In higher plants, cells contain hundreds of physically discrete mitochondria that are highly dynamic, predominantly moving on the actin cytoskeleton (Logan, 2010). Mitochondrial dynamics, including fission and fusion events, are expected to contribute to mitochondrial quality by promoting the exchange of components and ensuring organelles distribution throughout the cell to facilitate interaction with other organelles and metabolite exchanges. Recent quantitative analysis suggests that the costly mitochondrial dynamics is an inevitable trade-off that combines the organelles' motility with "social" contacts (Chustecki et al., 2021). Interestingly, in Arabidopsis seeds, mitochondria were found to remain static during imbibition until conditions promoting germination led to a reorganization of the chondriome around the nucleus as a network, followed by a general fragmentation at the end of germination that restored the typical mitochondrial dynamics (Paszkiewicz et al., 2017). Here, we have shown that mitochondrial dynamics were completely blocked following the heat shock treatment, albeit recovering in a few hours in the primed seedlings but not in the non-primed (H) seedlings (Figure 13). This temporary (or irreversible) blockage of mitochondrial dynamics is correlated with that of the actin network and ER, whose movements are also associated with actin microfilaments. However, the loss of mitochondrial dynamics upon heat shock differs from the lack of mobility observed in imbibing seeds, where the actin network was dynamic (Paszkiewicz et al., 2017). Although the effect of high temperature on plant mitochondria dynamics has received little attention, it could correlate to temperature conditions promoting cell death, like the exposure of protoplasts to a short acute heat shock (Scott & Logan, 2008). A cardiolipin-deficient Arabidopsis line, showing a defect in mitochondrial fission leading to "giant" mitochondria, was also susceptible to acute heat stress, leading to cell death (Pan et al., 2014). Recently, an Arabidopsis mutant hypersensitive to long-term heat stress (37°C, 5 days) was identified as deficient in ELM1, a component of the mitochondrial fission machinery, resulting in abnormal elongated mitochondria (Tsukimoto et al., 2022). Interestingly, wild-type plants treated with a myosin ATPase inhibitor were also found to be more heat sensitive, supporting the role of mitochondrial fission in heat tolerance. However, mitochondrial dynamics were not evaluated in these two studies. Whether the arrest of mitochondrial dynamics caused by the noxious heat shock is due solely to the arrest of the actin network dynamics remains to be determined. Other effects, such as the shortage of ATP, could hamper the movements of the actin network or other organelles. Indeed, the ATP level was recently shown to be coordinated with actin dynamics through the TORC1 (target of rapamycin complex 1) complex (Dai et al., 2022). It is noticeable that although respiration of the primed seedlings (PH condition) was decreased by around 40% at the end of the heat shock, organelle (mitochondria, ER, actin network) dynamics were blocked, which suggests that the energy status (e.g., ATP/ADP ratio) was too low to maintain dynamics. In the following hours of recovery, respiration and organelle dynamics recovered rapidly, supporting a functional link.

Heat shock response

Following heat sensing by mechanisms still under debate and investigation, plants build the multigenic HSR triggered at the transcriptional level by a battery of HSFs that induce the expression of various proteins involved in metabolism, anti-oxidative stress, and proteostasis, such as several HSPs which should be more precisely called heat-induced chaperones (Guihur et al., 2022). For biophysical reasons, temperature directly influences membrane fluidity and is thus expected to be a primordial factor for temperature sensing, mainly by activating cyclic nucleotide-gated calcium channels (Bourgine & Guihur, 2021; Guihur et al., 2022). Sessile plants can progressively adapt their membrane lipid composition when the temperature changes to adjust fluidity (so-called homeoviscous adaptation), but the process is slow (Falcone et al., 2004). It is, therefore, unlikely to occur in our conditions of priming or heat shock. Still, the increase in fluidity, especially in the case of the harmful heat shock, must have a substantial impact on membrane function including those of mitochondria and chloroplasts. Since heat stress compromises the structure and stability of many polypeptides, reinforcing the proteostasis machinery is crucial, and heat-induced molecular chaperones are, therefore, significant components of the HSR. Accordingly, we found that many chaperones were accumulating in primed seedlings in several compartments (Figure 12). Besides unfoldases and disaggregases (HSP70, HSP90, HSP101), sHSPs were strongly induced in the cytosol, mitochondria, and chloroplasts. The sHSPs are small proteins sharing the α--crystallin domain, which can assemble in large dynamic oligomers, and which are expected to bind unfolded proteins to prevent their irreversible aggregation and facilitate the work of other chaperones (unfoldases, disaggregases) under proteotoxic stress (Waters & Vierling, 2020). The observation that the cytosolic HSP17.6, plastidial HSP21, and mitochondrial HSP26.5 were found in the insoluble fraction during the heat shock supports their potential role as holdases co-precipitating with unfolded polypeptides.

However, the sHSP family is very diverse, and it remains unclear whether all sHSPs have similar functions. For instance, HSP17 from cyanobacteria was shown to also interact and stabilize thylakoid membranes (Török et al.,

2001), and in Arabidopsis, a large proportion of HSP21, a soluble protein of the stroma, was found to associate with thylakoids under heat stress (Bernfur et al., 2017). Therefore, HSP21 that accumulates upon priming could have a role to counteract the increase in membrane fluidity under heat shock, stabilizing membranes and thus explain the rather good protection of photosynthesis observed under PH conditions. HSP21 could have pleiotropic effects since it was also shown to associate with the plastidial transcription complex under heat stress (Zhong et al., 2013). With its multiple potential functions, HSP21 could therefore be a significant component of thermotolerance in the chloroplast, at least in higher plants, since it was only slightly induced by a heat priming treatment in the moss *Physcomitrium patens* (Guihur et al., 2020). In mitochondria, besides the increase of an HSP70 member (HSC70C), the priming treatment strongly induced the three sHSPs (HSP23.5, HSP23.6, HSP26.5), suggesting a protective role during heat shock and recovery. Mitochondrial sHSPs were ascribed various functions as molecular chaperones or as protectants of oxidative phosphorylation during heat or salt stress (Avelange-Macherel et al., 2020; Downs et al., 1999; Downs & Heckathorn, 1998; Hamilton III & Heckathorn, 2001; Heckathorn et al., 1999). In plants exposed to moderate heat stress (30°C), HSP23.6 was recently found to be strongly associated with membranes and to be a substrate of the proteases FTSH4 and OMA1 (Maziak et al., 2021). Simultaneous knock-down of the three mitochondrial sHSP genes in Arabidopsis led to a strong developmental phenotype (small chlorotic plants), leading to the hypothesis that these proteins are essential for vegetative and reproductive growth (Escobar et al., 2021). However, such a strong phenotype in the knock-down lines is surprising, considering that these proteins are almost essentially expressed during seed development and in response to heat stress. Another work about the cotton mitochondrial HSP24.7, which was extended to Arabidopsis and tomato, led to the proposal that temperature-dependent variations in mitochondrial sHSP abundance during germination would interfere with cytochrome *c*/*c1* biogenesis, leading to an increase in ROS production and the AOX pathway, promoting germination at warm temperature (Hu et al., 2019). However, this does not fit with the fact that pea seed mitochondria contain high amounts of HSP22, have almost no alternative oxidase activity, and the seeds germinate even at 0°C (Stupnikova et al., 2006). Moreover, during Arabidopsis seed imbibition and germination, respiration occurs through the cytochrome pathway to provide the high amount of ATP required, while the AOX pathway is engaged later (Réthoré et al., 2019). More research will thus be needed to clarify the physiological role of mitochondrial sHSP in heat-stressed tissues and seeds, and more generally about the clients of the sHSP chaperones. Indeed, an in-depth quantitative proteomics approach of the effect of a mild heat priming on *Physcomitrium patens* revealed that the strong fold change of sHSPs, which is emblematic of the HSR, represents only a modest proportion (4%) of the mass of the heat-accumulated proteins (Guihur et al., 2020). In other words, even after a striking induction, the absolute abundance of sHSPs remains low. Instead of a general role in proteostasis, this rather suggests that sHSPs would target rare proteins, such as specialized signaling proteins like those controlling cellular death pathways. A crucial question that will need to be explored by interactome and biochemical studies is how specific clients can be recognized among populations of unfolded or misfolded polypeptides. Whatever their individual roles, it makes little doubt that the accumulation of HSPs in several cellular compartments upon priming is a critical determinant of heat acclimation since these proteins cannot be induced under heat shock (Figure 13). This lack of induction is presumably due to the blockage of translation since, for many of these genes, a substantial increase in transcript level was observed under heat shock conditions.

A specific response to the combination of priming and heat shock

The overall results indicate that the primed PH seedlings withstand the toxic heat shock because they have already built an adapted molecular response that controls seedlings and cannot elaborate during the high-temperature treatment. Hence, P and PH seedlings display similar profiles in the molecular analyses. Still, hundreds of genes were found to be specifically up or downregulated at the transcriptional level in the PH condition. Upregulation involved many genes related to photosynthesis and mitochondrial RNA editing, which is intriguing since heat stress is known to lower the efficiency of chloroplast and mitochondria RNA editing efficiency (Castandet et al., 2016; Zhang et al., 2020). This lowered efficiency was proposed to favor the expression of the non-edited targeted genes (less efficient proteins in optimal conditions) in a general context of lowered translation, which would represent a trade-off between quantity and quality (Chu & Wei, 2020). The increase of transcripts encoding editing actors that we observed could also be a player in this trade-off. However, to fully explain the contribution of organellar RNA edition in heat acclimation, it would be necessary to investigate further kinetics of expression of genes encoding the editing machineries during PH treatment and recovery, but also to quantify the rate of edition for the target RNAs, and ideally how their translation is affected. UBP1B, an RNA-binding protein that was localized in stress granules (Weber et al., 2008), increased by almost threefold, specifically in the PH condition. Mutant and overexpressing lines revealed that UBP1B was increasing thermotolerance of Arabidopsis, and micro-array analysis identified hundreds

of genes whose expression was raised in the overexpressing lines, under control or heat stress conditions, a likely consequence of prevention of RNA decay (Nguyen et al., 2016). In our experimental setup, since translation is expected to be blocked at 43°C (Echevarría-Zomeño et al., 2016; Yángüez et al., 2013), this increase in UPB1B occurred during the 2 h of recovery (which preceded sampling for proteomics), supporting a crucial role of the protein in maintaining high levels of essential mRNAs that would otherwise be degraded, during heat stress but also early recovery. Finally, it must be recalled that the overall protein turnover in mitochondria from Arabidopsis cell culture or seedlings is slow, with a median value of half-life of around 9 days (Huang et al., 2020). In hydroponically grown seedlings, the shortest half-life measured among 455 proteins was 34 h (Li et al., 2017). It would thus be of great interest to quantify mitochondria (and chloroplast) protein turnover following priming and heat shock to better understand how these organellar proteomes, which are globally very stable, are maintained and repaired.

Does priming inhibit heat-induced programmed cell death?

It is noticeable that more than 5 days after heat shock are needed for the H seedlings to start displaying visible symptoms of death, like the loss of chlorophyll. In the same period, after the major reduction observed just after the heat shock, respiration remained stable, while photosynthesis slowly decreased after the second day. H seedlings thus remain alive long after the heat shock, and therefore, their death is not the consequence of the acute heat increase but rather results from a controlled mechanism. While programmed cell death (PCD) mechanisms have been extensively investigated in animals, the knowledge about the process in plants lags, although several key actors have been either identified or shown to function when ectopically expressed in plants (Kabbage et al., 2017). In the PH seedlings, while protection of energy metabolism, thermosensitive membranes, and proteins is mandatory, the control of mechanisms related to cell death could be equally important. In animals, it is now well established that molecular chaperones and other proteins induced by the activation of HSFs (in particular HSFA1) also counteracts apotosis as well as other forms of PCD by interacting with various signaling actors (Zhang et al., 2021). Although much less in known in plants, similar functions could be expected, as discussed above about the sHPS which could possibly target signaling proteins of low abundance. For instance, seven genes belonging to the Bcl-2 associated anthanogen (BAG) family, whose most human members are anti-apoptotic, were identified in Arabidopsis and are now considered as key regulators of plant PCD (Doukhanina et al., 2006; Kabbage et al., 2017). BAG proteins are co-chaperones of HSP70/HSC70, and some plant members can also interact with calmodulin, suggesting a role in calcium signaling (Jiang et al., 2023). Interestingly, AtBag5, which was shown to be localized to mitochondria, was also demonstrated to associate with HSC70 and calmodulin into a signaling complex preventing senescence (Li et al., 2016). We found that *AtBAG5* (*At1G12060*) and *AtBAG6* (*At2G46240*) transcripts were highly overexpressed in P, H, and PH conditions (Table S1), which confirms a role in heat stress tolerance for the latter as deduced from the *bag6* mutant characterization (Arif et al., 2021). However, because the transcripts are upregulated in the three conditions and since the proteins could not be detected in the shotgun proteomics, further investigation is needed to uncover a possible role of these genes in the regulation of PCD in our system. In human cells, but also Arabidopsis, heat-induced death can also occur through a so-called ferroptosis-like cell death, whose hallmarks are the depletion of glutathione and accumulation of soluble and lipid reactive oxygen species (Distéfano et al., 2017). In this work, seedlings grown on MS plates and exposed to a heat shock (43°C, 1 h) displayed leaf whitening within 3 days but were significantly protected by pre-treatments with iron chelators or dipheniliodionium, which suggested the involvement of a ferroptosis pathway, likely involving the *KISS OF DEATH* (*KOD*) gene. KOD was identified earlier as an inducer of heat-induced PCD through the depolarization of mitochondria (Blanvillain et al., 2011). Although *KOD* is not annotated in the Arabidopsis genome, the RNAseq data revealed that this gene was exclusively expressed in H and PH samples, albeit at low and similar levels (9.0 ± 2.6 and 8.3 ± 2.1 transcript per million, respectively), which do not argue strongly in favor of a role of KOD and/or ferroptosis in the delayed death of the H seedlings. Clearly, a dedicated study with more detailed kinetics after the heat shock will be required to explain the slow death of the seedlings and understand the effects of priming on signaling pathways.

Concluding remarks

In the environment, plants must rapidly learn how to cope with critical conditions such as severe heat stress. Although seedlings are generally considered fragile and highly stress-sensitive, we show here that they rapidly build upon priming at 38°C an orchestrated response to cope, the day after, with a noxious 43°C heat shock. While the primary signature of this acclimation process remains the HSR, with the induction of molecular chaperones to counteract the destabilization of proteins and membranes, the protection of energy metabolism during heat stress and its fast and complete restoration during recovery was shown to be critical. Upon stress relief, mitochondria and chloroplast provide the energy required to rapidly restore normal metabolism and cellular mechanisms, as illustrated

by organelle dynamics. In the absence of priming, structures are damaged by excessive heat, and energy transduction is compromised, paving the way toward cell death. Still, this large-scale study will need additional experiments, in particular with more time points, to strengthen the conclusions regarding organelle maintainance, and clarify the function of the many molecular changes that were identified.

EXPERIMENTAL PROCEDURES

Plant material and heat stress regimes

All experiments were conducted using the *Arabidopsis thaliana* Columbia ecotype (Col-0). Visualization of mitochondria was performed using a Mito-GFP transgenic line, (Logan & Leaver, 2000), of endoplasmic reticulum (ER) with the ER-gk CS16251 line (Nelson et al., 2007) and of actin with the GFP-Lifeact line (Garagounis et al., 2017; Riedl et al., 2008). Seedlings were grown according to (Réthoré et al., 2019). After 2 h of photoperiod, heat stress treatments were realized by transferring seedlings with their medium (5 ml) into 25 ml glass bottles (Schott Duran, Sigma-Aldrich, Saint Louis, USA) and placing them for 2 h in a water bath set up at a defined temperature. This method allowed the presence of enough air in the medium to avoid hypoxia during stress. Priming was performed at 38°C and heat shock at 43°C (Figure 1). Two LED ramps (Starlicht 563 539 345 Armature StarLED Senzo Dim 50, www.amazon.fr) ensured illumination during heat treatments at a PAR intensity similar to that used in the growth room (150 μmol photons m^{-2} sec^{-1}). After treatment, seedlings were transferred back into the six-well plates in the growth room for recovery. For green pixel detection, plates were imaged with a Nikon D5000 during the days following heat shock (Nikon France SAS, Champigny sur Marne, France) with a single lens reflex camera equipped with a 60 mm Nikkor microlens, using a stand. The analysis was performed with ImageJ software using a previously developed macro (Benamar et al., 2013).

Oxygen measurement

Measurements of oxygen exchange in 1 ml of Evian natural mineral water containing around 50 mg of seedlings were performed using an Oxygraph electrode system (Hansatech, King's Lynn, UK) calibrated at 25, 38, or 43°C with maximum stirring speed. A halogen cold light source with two fibers, VisiLight CL150 (VWR, Radnor, USA), was used for photosynthesis measurement. It was calibrated at a saturating light of around 800 μmol photons.m^{-2}.sec^{-1} (400 for each fiber) using QRT1 Quantitherm (Hansatech) as a light calibration system. Respiration was assessed during the second period of dark after maximal net photosynthesis measurement with the saturating light. Rates were standardized using the total chlorophyll amount in each experiment. Seedlings were recovered, and pigments were extracted in 1 ml of dimethylformamide at 4°C for at least 24 h. Absorbance at 647 and 664 nm was measured from 100 μl of supernatant using a Quartz plate and a FLUOstar Omega (BMG Labtech, Ortenberg, Germany) spectrophotometer. The total amount of chlorophyll (a+b) was calculated according to (Moran, 1982) using the formula: total chll = 7.04 A664 + 20.27 A647 (in μg).

Chlorophyll fluorescence

Seedlings were dark-adapted for 30 min before the acquisition of chlorophyll fluorescence. Images of chlorophyll fluorescence from six-well plates were acquired using a PSI Open FluorCam FC 800-O (PSI, Brno, Czech Republic) and a 12-bit dynamic CCD camera with a 512 × 512 pixel resolution. The system included four LED panels divided into two pairs. One pair provided an orange actinic light with a wavelength of 618 nm, with variable intensity (200–400 μmol m^{-2} sec^{-1}). The other pair provided a saturating pulse at 455 nm during 0.8 sec, with an intensity of up to 3000 μmol m^{-2} sec^{-1}. The saturating pulse allowed the collection of the maximum fluorescence (Fm) after measurement of F0 acquisition in the dark-adapted mode. Maximum photosystem II quantum yield was calculated using Fv/Fm, in which Fv = Fm-F0.

Live cell imaging

Live cell epifluorescence microscopy was performed using a Zeiss Axio Imager Z2 microscope driven by ZEN software (Carl Zeiss SAS, Rueil-Malmaison, France) with 100× Zeiss Plan-Apochromat oil immersion objective (NA 1.4) for mitochondrial and ER dynamics. Excitation filter 450–490 m (using LED module 470 nm) and emission filter 500–550 nm were used for GFP fluorescence. For actin dynamics, confocal laser scanning microscopy (CLSM) was performed using a Nikon A1 microscope driven by NIS Elements software (Nikon) using Nikon CFI Apo 40× WI objective (NA 1.25). Excitation and emission wavelengths were 488 and 500–550 nm, respectively. Images were acquired on at least two different areas of the same seedling and at least three different seedlings.

Quantification of organelle dynamics

For mitochondria and ER, stacks of images (66.56 × 66.56 μm) were captured at 2 sec intervals for 20 sec, with an image size of 1024 × 1024 pixels, giving a pixel size of 0.065 μm. Stacks were processed using IMARIS v8.2 (Oxford Instruments, Abingdon, Oxfordshire, UK) to enable object identification, tracking, and calculation of track speed. Object reconstruction was performed by automatic thresholding using background subtraction (rolling ball of 0.3 μm). Tracking over time was performed using the autoregressive motion algorithm. ER time stacks were processed using Fiji (Schindelin et al., 2012) to filter noise (Gaussian Blur and background subtraction) and to superimpose two images (25 × 25 μm) of the same field of view captured 20 sec apart. Colocalization analysis of these two images was performed using Pearson's correlation coefficient calculated by Coloc 2 plug-in using the Costes method (Costes et al., 2004). For actin, stacks of images (147.13 × 147.13 μm) were captured at 12 sec intervals for 3 min, with an image size of 1024 × 1024 pixels, giving a pixel size of 0.144 μm. Stacks were processed using Fiji (Gaussian blur: 1 and subtract background: 20), and two images (50 × 50 μm) of the same field-of-view captured 2 min apart were superimposed. Colocalization analysis of these two images was performed using Pearson's correlation coefficient calculated by Coloc 2.

Transcriptomic analysis

Transcriptomic analysis was performed on triplicate samples corresponding to four different conditions: C and P after 30 min of 38°C treatment, H and PH after 30 min of 43°C treatment using control and primed seedlings, respectively. Around 100 mg of seedlings were ground in liquid nitrogen using a mortar and pestle. RNA extraction was performed using the NucleoSpin RNA Plus kit, following manufacturer instructions (Macherey Nagel, Düren, Nordrhein-Westfalen, Germany). A step of on-column DNA digestion was added after the first step of washing with buffer WB1 using 80 μl DNase RNase-free (QIAGEN, Courtaboeuf, France). RNA quality was checked using an Experion automated electrophoresis system (Bio-Rad, Marnes-le-Coquette, France): all 28S:18S ratios were

over 1.5 and RQI >8.5. Ribosomal RNAs were removed using an RNA depletion kit before cDNA library construction and sequencing using strand-specific long non-coding RNA Illumina HiSeq™ 4000 sequencing with a paired-end read-length of 100 bp (BGI, Hong Kong). Clean reads (>80 M reads of 100 bp per sample) were aligned to the Arabidopsis transcriptome (TAIR10) using Bowtie2 and SAMtools packages. DESeq2 package was used for differential analysis. Transcripts presenting FDR <0.05 and a log2 ratio >1 or <−1 between two conditions were considered as significantly upregulated or downregulated, respectively. Subcellular annotation of proteins was performed according to the SUBAcon predictor from the SUBA 4 database (Hooper et al., 2014, 2017). Venn diagrams were realized using Intervene software (Khan & Mathelier, 2017). The RNAseq data discussed in this publication have been deposited in NCBI's Gene Expression Omnibus (Edgar, 2002) and are accessible through GEO Series accession number GSE236157 (https://www.ncbi.nlm.nih.gov/geo/query/acc.cgi?acc=GSE236157).

Proteome analysis

Proteomic analysis was performed on four replicates, corresponding to four different conditions: C, P just before heat shock, H and PH 2 h after heat shock, using control and primed seedlings, respectively. Samples of around 200 mg seedlings were ground with two glass beads (3 mm) using a TissueLyser (Qiagen, Hilden, Germany) at 30 Hz for 1 min. The powder was suspended using 1.2 ml of 10% TCA/0.07% β-mercaptoethanol/cold acetone at −20°C for 1 h. After centrifugation for 20 min at 20 000 ***g*** at 4°C, the pellets were rinsed three times with cold acetone/0.07% β–mercaptoethanol. Pellets were then dried using a miVac QUATTRO concentrator (SP Scientific, Ipswich, UK) and solubilized in a buffer containing 6 M Urea, 2 M thiourea, 30 mM Tris pH 8.8, 10 mM dithiothreitol (DTT) and 0.1% ZALS (zwitterionic acid-labile surfactant, Proteabio, Morgantown, WV, USA) dissolved in 50 mM ammonium bicarbonate, using 22 µl per mg of pellet. After centrifugation (20 000 ***g***; 20°C) for 20 min, the supernatant was recovered and kept at −80°C until proteomic analysis, which was performed at the PAPPSO facility (INRA, Le Moulon, Gif sur Yvette). Protein concentration was determined using Plus One 2D QuantKit (Amersham) and bovine serum albumin (BSA) as a standard. Using 25 µg proteins, reduced cysteine groups were alkylated by incubation in 50 mM iodoacetamide (IAA) in darkness. The protein mixture was diluted to 1:10 in 50 mM ammonium bicarbonate pH 8, to reduce the concentration of urea to less than 1 M. 600 ng trypsin was added to digest protein at 37°C overnight. Digestion was stopped with trifluoroacetic acid (TFA, final concentration of 1%). Samples were desalted (15 µg) using 96 well Strata™XL 100 µm Polymeric Reversed Phase Plates (Phenomenex, Le Pecq, France). Desalted samples were solubilized in 0.1% (v/v) formic acid (FA) and 2% acetonitrile (v/v) (ACN) and were analyzed on a HPLC/nanoRSLC Orbitrap tribid Fusion Lumos (Thermo Fisher) spectrometer. Loading buffer contained 2% ACN and 0.08% (v/v) TFA. Buffer A was prepared with 2% ACN and 0.1% FA and buffer B with 80% ACN and 0.1% FA. 800 ng of proteins were loaded on a 0.3 × 5 mm pre-column with a particle size of 5 µm and a pore size of 100 Å (PepMap 100 C18, Thermo Fisher Scientific, Waltham, MA, USA) and rinsed for 5 min at 20 µl. min^{-1}. Samples were then separated on a 75 µm × 500 mm column with a particle size of 3 µm and a pore size of 100 Å (Acclaim PepMap 100 C18, Thermo Fisher) using a flow of 300 nl min^{-1}, at 40°C, according to the following gradient (buffer B in buffer A): 1 to 6% from 0 to 3 min; 6 to 28% from 3 to 160 min; 40 to 98% 180 to 185 min; 98% from 185 to 195 min; 98 to 6% 195 to 197 min; 6 to 1% 197 to 202 min. Ionization (at 1600 V) and capillary transfer (275°C) were performed using a liquid junction and a capillary probe (SilicaTip™ Emitter, 10 µm, New Objective). Peptide ion analysis was realized with Xcalibur software (Thermo Fisher). The Full MS Orbitrap was set up with a resolution of 120 000, a scan range of 350–1400 m/z, an AGC target of 5e5, a maximum injection time of 54 ms, a profile data type, and an RF lens of 30%. Parameters for precursor selection were set as follows: TOP speed, 2 sec; analyzed charge states, 2–4; intensity threshold, 1e4; dynamic exclusion, 60 sec; mass precision, ±10 ppm. For MS/MS, the AGC target was 5e4, the maximum injection time was 80 ms, and the fragmentation mode was HCD with a collision energy of 27% and a resolution of 30 000.

Raw data were converted to mzXML open format using Proteowizard 3.0.9205 (Kessner et al., 2008). Protein identification and filtering were performed using X!Tandem Alanine (2017.2.1.4) (Craig & Beavis, 2004) and X!Tandem Pipeline 3.4.3 (Langella et al., 2017) by querying MS/MS data against the TAIR10 database together with a custom contaminant database (trypsin, keratins). Identified proteins were filtered and grouped using X! Tandem Pipeline according to two criteria: (1) a minimum of two different peptides required with an E-value smaller than 0.01, and (2) a protein E-value (calculated as the product of unique peptide E-values) smaller than 10^{-5}. The false discovery rates (FDRs) at the peptide and protein levels were 0.14 and 0.2%, respectively. Relative peptide quantification by peak-area integration on eXtracted ion chromatogram (XIC) was performed using the MassChroQ software (pappso.inra.fr/bioinfo/masschroq/) (Valot et al., 2011); Peptides shared by two or more proteins were removed. Peptides that had more than 10% of missing data were considered unreproducible and removed. Peptides whose intensity profiles deviate from the average profile of the peptides belonging to the same protein (with a coefficient of correlation inferior to 0.5) were also removed. The minimal number of peptides per protein was set to 2. Relative protein abundance was calculated and defined as the sum of peptide intensities considering only (1) reproducible peptides, (2) specific peptides, and (3) correlated peptides belonging to the same protein. Statistical analysis was performed using ANOVA and Tukey's test (glht function of the multcomp *R* package). When the peptides of a protein were not present or not reproducibly observed in one or more conditions, spectral counting (SC) with a minimum number of spectra set to 5 was used in place of XIC analysis. Statistical analysis of SC was performed using ANOVA on a glm model (Poisson family) and chi-squared test. Venn diagrams were performed using Venny2.0 (Oliveros, 2007). The mass spectrometry proteomics data have been deposited to the ProteomeXchange Consortium via the PRIDE (Perez-Riverol et al., 2022) partner repository with the dataset identifier PXD045392.

Metabolic profiling

Samples were collected just before heat shock (C and P d0) or just after (H+0 h and PH+0 h) and after 2 h (H+2 h and PH+2 h) or 24 h recovery (C, P, H, and PH d+1). Triplicates of around 200 mg seedlings were lyophilized and ground with two glass beads (3 mm) using TissueLyser (Qiagen) at 30 Hz for 1 min. Polar metabolites were extracted according to (Réthoré et al., 2019). Alpha-aminobutyric acid, phthalic acid, and melezitose were used as internal standards for amino acids, organic acids, and sugars, respectively. Samples were derivatized and analyzed according to Réthoré et al. (2019). Heatmaps were performed using MetaboAnalyst 4.0 with the Euclidian distance method and ward clustering algorithm after Pareto scaling (Chong et al., 2018).

Western blot

Seedlings were sampled after 0, 30, 60, and 120 min of heat treatment (38°C or 43°C with or without previous acclimation)

and after 2, 4, 6 h, or 1–10 days of recovery. Protein extraction and western blot analysis were performed according to Réthoré et al. (2019). All antibodies were purchased from Agrisera (Vännäs, Sweden). Anti-HSP101 (AS07253), anti-cytosolic HSP70 (AS08371) and anti-HSP17.6 (AS07254) antibodies were diluted to 1:3000, and anti-chloroplastic HSP70 (AS08348), anti-HSP21 (AS08285), anti-HSP26.5 (AS152981) to 1:1000. Secondary antibody (goat anti-rabbit IgG horse radish peroxidase conjugated, AS09602) was diluted to 1:75000. Total proteins were visualized on the membranes using UV detection (Stain Free technology, Bio-Rad), before developing membranes for 5 min with Western Clarity ECL (Bio-Rad), using a ChemiDoc XRS+ imaging system (Bio-Rad). Semi-quantification of HSPs on western blots was performed using the normalization tool of ImageLab software (Bio-Rad): RbcL protein was used as a reference band on stain-free images for normalization of chemiluminescence signals. For each protein, intensities in each sample were expressed as the percentage of maximal intensity detected on the same membrane.

For immunodetection of HSPs remaining in the tissue pellets after protein extraction, 100 µl of 5X Laemmli buffer and 400 µl grinding buffer were added to the pellet. After vortex and centrifugation, the supernatant was transferred to a new tube and processed as above. 30 µl of each protein extract was loaded on 12% Stain Free Gels (Bio-Rad) and immunodetection was performed as described above.

Statistics and data analysis

Unless otherwise stated, statistical analysis was performed using a *t*-test or ANOVA followed by the Tukey test ($P < 0.05$) in SigmaPlot v11.0 software (Systat Software Inc., Chicago, IL, USA). The sparse partial least squares discriminant analysis (sPLS–DA) was performed with the mixOmics R package v.6.26.0 (Rohart et al., 2017) following the guidelines provided on its website (http://mixomics.org/case-studies/splsda-srbct-case-study). The transcriptomic and proteomic data were analyzed separately. The differentially expressed transcripts subset and the whole proteins data (XIC measurements) were used for the analysis. The sPLS–DA model was tuned several times with fivefold cross-validation repeated 50 times to set the maximum number of components and the optimal number of variables to select for each component. For the transcriptome set, the tuning function consistently indicated that the optimal number of components was three and the optimal number of classification variables for components 1, 2, and 3 were 1, 60, and 30, respectively. For the proteome set, the optimal number of components was 2 and the optimal number of classification variables for components 1 and 2 were 1 and 60, respectively. Whenever the sPLS–DA tuning indicated only one variable, we extended this number to 10 to gain in biological interpretation. Selected transcripts and proteins were extracted from final sPLS–DAs, according to their contribution to subgroup discrimination in a given component (loading weight). Graphs were drawn with Metaboanalyst v6.0 (https://www.metaboanalyst.ca/MetaboAnalyst/home.xhtml) after repeating the sPLS–DA with the tuned parameters determined by mixOmics *R* package. The functional relevance of the most discriminative genes and proteins was explored using AgriGo v2.0 (Tian et al., 2017). Differentially expressed proteins in P, H, and PH conditions compared to control (XIC quantification, ANOVA, and Tukey test $P < 0.05$) were analyzed for prediction of associations by STRING version 12.0 (https://string-db.org/) (Szklarczyk et al., 2019) with the following settings: full string network, confidence (medium confidence of 0.7) and MCL clustering (inflation parameter of 1.5).

ACKNOWLEDGMENTS

We are thankful to Abdelilah Benamar and Daniel Beucher (plant culture and physiology), Fabienne Simonneau and Aurélia Rolland (IMAC-QUASAV, confocal microscopy), Pascale Satour and Caroline Cukier (IRHS-SMS, metabolic analysis) and Martine Neveu (western blot analysis). We are grateful to Sylvain Gaillard for his assistance in RNA-seq analysis and to Alain Bouchereau for discussions about metabolism. We also would like to thank Lee J. Sweetlove for kindly providing us with the GFP-Lifeact line. This research was conducted in the framework of the regional program "Objectif Végétal, Research, Education and Innovation in Pays de la Loire," supported by the French Region Pays de la Loire, Angers Loire Métropole and the European Regional Development Fund.

AUTHOR CONTRIBUTIONS

ER, MHAM and DM designed the research project and wrote the manuscript; ER, MHAM, TB, and DM performed experiments. SP, TB, and MZ contributed to transcriptomic and proteomic data treatment and analysis. All authors read and agreed with the manuscript.

CONFLICT OF INTEREST

The authors declare no conflict of interest.

SUPPORTING INFORMATION

Additional Supporting Information may be found in the online version of this article.

Figure S1. Impact of heat stress on maximum photosystem II quantum yield.

Figure S2. Rapid recovery of mitochondrial dynamics in response to heat stress at 43 °C for primed seedlings (PH condition).

Figure S3. Evolution of endoplasmic reticulum dynamics in response to heat stress.

Figure S4. sPLS–DA analysis of transcripts.

Figure S5. sPLS–DA analysis of proteins.

Figure S6. HSPs detected by XIC and spectral counting (SC).

Figure S7. Semi-quantitative analysis of HSP protein levels detected in P, H, and PH samples during and after treatment.

Table S1. Total list of transcripts analyzed in response to P, H, or PH after 30 min of treatment.

Table S2. Results of sPLS–DA analysis of transcripts.

Table S3. Total list of proteins analyzed in response to P, H, or PH after 2 h of recovery post-treatment according to XIC analysis.

Table S4. STRING analysis of differentially expressed proteins in P, H, and PH conditions.

Table S5. Results of sPLS–DA analysis of proteins.

Table S6. Evolution of amino acids, organic acids, and sugar contents in response to priming and heat shock.

OPEN RESEARCH BADGES

This article has earned an Open Data badge for making publicly available the digitally-shareable data necessary to reproduce the reported results. The data is available at GEO accession number GSE236157 (https://www.ncbi.nlm.nih.gov/geo/query/acc.cgi?acc=GSE236157). PRIDE (https://www.ebi.ac.uk/pride/) identifier PXD045392.

DATA AVAILABILITY STATEMENT

All relevant data can be found within the manuscript and its supporting material.

REFERENCES

Ahuja, I., **de Vos, R.C.H.**, **Bones, A.M.** & **Hall, R.D.** (2010) Plant molecular stress responses face climate change. *Trends in Plant Science*, **15**, 664–674.

Allakhverdiev, S.I., **Kreslavski, V.D.**, **Klimov, V.V.**, **Los, D.A.**, **Carpentier, R.** & **Mohanty, P.** (2008) Heat stress: an overview of molecular responses in photosynthesis. *Photosynthesis Research*, **98**, 541–550.

Arif, M., **Li, Z.**, **Luo, Q.**, **Li, L.**, **Shen, Y.** & **Men, S.** (2021) The BAG2 and BAG6 genes are involved in multiple abiotic stress tolerances in Arabidopsis thaliana. *International Journal of Molecular Sciences*, **22**, 5856.

Atkin, O.K. & **Tjoelker, M.G.** (2003) Thermal acclimation and the dynamic response of plant respiration to temperature. *Trends in Plant Science*, **8**, 343–351.

Avelange-Macherel, M.H., **Rolland, A.**, **Hinault, M.P.**, **Tolleter, D.** & **Macherel, D.** (2020) The mitochondrial small heat shock protein HSP22 from pea is a thermosoluble chaperone prone to co-precipitate with unfolding client proteins. *International Journal of Molecular Sciences*, **21**, 97.

Baker, N.R. (2008) Chlorophyll fluorescence: a probe of photosynthesis in vivo. *Annual Review of Plant Biology*, **59**, 89–113.

Belouah, I., **Blein-Nicolas, M.**, **Balliau, T.**, **Gibon, Y.**, **Zivy, M.** & **Colombié, S.** (2019) Peptide filtering differently affects the performances of XIC-based quantification methods. *Journal of Proteomics*, **193**, 131–141.

Benamar, A., **Pierart, A.**, **Baecker, V.**, **Avelange-Macherel, M.-H.**, **Rolland, A.**, **Gaudichon, S.** ***et al.*** (2013) Simple system using natural mineral water for high-throughput phenotyping of Arabidopsis thaliana seedlings in liquid culture. *International Journal of High Throughput Screening*, **4**, 1–15.

Bernfur, K., **Rutsdottir, G.** & **Emanuelsson, C.** (2017) The chloroplast-localized small heat shock protein Hsp21 associates with the thylakoid. *Protein Science*, **26**, 1173–1784.

Bita, C.E. & **Gerats, T.** (2013) Plant tolerance to high temperature in a changing environment: scientific fundamentals and production of heat stress-tolerant crops. *Frontiers in Plant Science*, **4**, 273.

Bitrián, M., **Zarza, X.**, **Altabella, T.**, **Tiburcio, A.F.** & **Alcázar, R.** (2012) Polyamines under abiotic stress: metabolic crossroads and hormonal crosstalks in plants. *Metabolites*, **2**, 516–528.

Blanvillain, R., **Young, B.**, **Cai, Y.**, **Hecht, V.**, **Varoquaux, F.**, **Delorme, V.** ***et al.*** (2011) The *Arabidopsis* peptide kiss of death is an inducer of programmed cell death: an *Arabidopsis* short peptide regulating PCD. *The EMBO Journal*, **30**, 1173–1183.

Bourgine, B. & **Guihur, A.** (2021) Heat shock signaling in land plants: from plasma membrane sensing to the transcription of small heat shock proteins. *Frontiers in Plant Science*, **12**, 710801.

Branco-Price, C., **Kaiser, K.A.**, **Jang, C.J.H.**, **Larive, C.K.** & **Bailey-Serres, J.** (2008) Selective mRNA translation coordinates energetic and metabolic adjustments to cellular oxygen deprivation and reoxygenation in *Arabidopsis thaliana*. *The Plant Journal*, **56**, 743–755.

Caldana, C., **Degenkolbe, T.**, **Cuadros-Inostroza, A.**, **Klie, S.**, **Sulpice, R.**, **Leisse, A.** ***et al.*** (2011) High-density kinetic analysis of the metabolomic and transcriptomic response of Arabidopsis to eight environmental conditions. *The Plant Journal*, **67**, 869–884.

Castandet, B., **Hotto, A.M.**, **Strickler, S.R.** & **Stern, D.B.** (2016) ChloroSeq, an optimized chloroplast RNA-Seq bioinformatic pipeline, reveals remodeling of the organellar transcriptome under heat stress. *G3: Genes, Genomes, Genetics*, **6**, 2817–2827.

Chen, K., **Gao, Y.**, **Mih, N.**, **O'Brien, E.J.**, **Yang, L.** & **Palsson, B.O.** (2017) Thermosensitivity of growth is determined by chaperone-mediated proteome reallocation. *Proceedings of the National Academy of Sciences*, **114**, 201705524.

Chong, J., **Soufan, O.**, **Li, C.**, **Caraus, I.**, **Li, S.**, **Bourque, G.** ***et al.*** (2018) MetaboAnalyst 4.0: towards more transparent and integrative metabolomics analysis. *Nucleic Acids Research*, **46**, W486–W494.

Chu, D. & **Wei, L.** (2020) Reduced C-to-U RNA editing rates might play a regulatory role in stress response of Arabidopsis. *Journal of Plant Physiology*, **244**, 153081.

Chustecki, J.M., **Gibbs, D.J.**, **Bassel, G.W.** & **Johnston, I.G.** (2021) Network analysis of Arabidopsis mitochondrial dynamics reveals a resolved trade-off between physical distribution and social connectivity. *Cell Systems*, **12**, 419–431.e4.

Ciais, P., **Reichstein, M.**, **Viovy, N.**, **Granier, A.**, **Ogée, J.**, **Allard, V.** ***et al.*** (2005) Europe-wide reduction in primary productivity caused by the heat and drought in 2003. *Nature*, **437**, 529–533.

Closa, M., **Vranová, E.**, **Bortolotti, C.**, **Bigler, L.**, **Arró, M.**, **Ferrer, A.** ***et al.*** (2010) The *Arabidopsis thaliana* FPP synthase isozymes have overlapping and specific functions in isoprenoid biosynthesis, and complete loss of FPP synthase activity causes early developmental arrest. *The Plant Journal*, **63**, 512–525.

Costes, S.V., **Daelemans, D.**, **Cho, E.H.**, **Dobbin, Z.**, **Pavlakis, G.** & **Lockett, S.** (2004) Automatic and quantitative measurement of protein-protein colocalization in live cells. *Biophysical Journal*, **86**, 3993–4003.

Craig, R. & **Beavis, R.C.** (2004) TANDEM: matching proteins with tandem mass spectra. *Bioinformatics*, **20**, 1466–1467.

Cunillera, N., **Boronat, A.** & **Ferrer, A.** (1997) The *Arabidopsis thaliana* FPS1 gene generates a novel mRNA that encodes a mitochondrial farnesyl-diphosphate synthase isoform. *The Journal of Biological Chemistry*, **272**, 15381–15388.

Dai, L., **Wang, B.**, **Wang, T.**, **Meyer, E.H.**, **Kettel, V.**, **Hoffmann, N.** ***et al.*** (2022) The TOR complex controls ATP levels to regulate Actin cytoskeleton dynamics in Arabidopsis. *Proceedings of the National Academy of Sciences of the United States of America*, **119**, 1–12.

Dell'Aglio, E., **Boycheva, S.** & **Fitzpatrick, T.B.** (2017) The pseudoenzyme PDX1.2 sustains vitamin B6 biosynthesis as a function of heat stress. *Plant Physiology*, **174**, 2098–2112.

Diamant, S., **Eliahu, N.**, **Rosenthal, D.** & **Goloubinoff, P.** (2001) Chemical chaperones regulate molecular chaperones in vitro and in cells under combined salt and heat stresses. *The Journal of Biological Chemistry*, **276**, 39586–39591.

Dickinson, P.J., **Kumar, M.**, **Martinho, C.**, **Yoo, S.J.**, **Lan, H.**, **Artavanis, G.** ***et al.*** (2018) Chloroplast signaling gates thermotolerance in Arabidopsis. *Cell Reports*, **22**, 1657–1665.

Distéfano, A.M., **Martin, M.V.**, **Córdoba, J.P.**, **Bellido, A.M.**, **D'Ippólito, S.**, **Colman, S.L.** ***et al.*** (2017) Heat stress induces ferroptosis-like cell death in plants. *The Journal of Cell Biology*, **216**, 463–476.

Doukhanina, E.V., **Chen, S.**, **Van Der Zalm, E.**, **Godzik, A.**, **Reed, J.** & **Dickman, M.B.** (2006) Identification and functional characterization of the BAG protein family in *Arabidopsis thaliana*. *The Journal of Biological Chemistry*, **281**, 18793–18801.

Downs, C.A. & **Heckathorn, S.A.** (1998) The mitochondrial small heat-shock protein protects NADH: ubiquinone oxidoreductase of the electron transport chain during heat stress in plants. *FEBS Letters*, **430**, 246–250.

Downs, C.A., **Jones, L.R.** & **Heckathorn, S.A.** (1999) Evidence for a novel set of small heat-shock proteins that associates with the mitochondria of murine PC12 cells and protects NADH:ubiquinone oxidoreductase from heat and oxidative stress. *Archives of Biochemistry and Biophysics*, **365**, 344–350.

Driedonks, N., **Xu, J.**, **Peters, J.L.**, **Park, S.** & **Rieu, I.** (2015) Multi-level interactions between heat shock factors, heat shock proteins, and the redox system regulate acclimation to heat. *Frontiers in Plant Science*, **6**, 999.

Echevarría-Zomeño, S., **Fernández-Calvino, L.**, **Castro-Sanz, A.B.**, **López, J.A.**, **Vázquez, J.** & **Castellano, M.M.** (2016) Dissecting the proteome dynamics of the early heat stress response leading to plant survival or death in Arabidopsis. *Plant, Cell & Environment*, **39**, 1264–1278.

Edgar, R. (2002) Gene expression omnibus: NCBI gene expression and hybridization array data repository. *Nucleic Acids Research*, **30**, 207–210.

Elrouby, N. & **Coupland, G.** (2010) Proteome-wide screens for small ubiquitin-like modifier (SUMO) substrates identify Arabidopsis proteins implicated in diverse biological processes. *Proceedings of the National Academy of Sciences of the United States of America*, **107**, 17415–17420.

Escobar, M.R., **Feussner, I.** & **Valle, E.M.** (2021) Mitochondrial small heat shock proteins are essential for normal growth of *Arabidopsis thaliana*. *Frontiers in Plant Science*, **12**, 1–20.

Fahad, S., **Bajwa, A.A.**, **Nazir, U.**, **Anjum, S.A.**, **Farooq, A.**, **Zohaib, A.** ***et al.*** (2017) Crop production under drought and heat stress: plant responses and management options. *Frontiers in Plant Science*, **8**, 1–16.

Falcone, D.L., **Ogas, J.P.** & **Somerville, C.R.** (2004) Regulation of membrane fatty acid composition by temperature in mutants of Arabidopsis with alterations in membrane lipid composition. *BMC Plant Biology*, **4**, 1–45.

Fan, T., **Wang, R.**, **Xiang, Y.**, **An, L.** & **Cao, S.** (2016) Heat stress induces Actin cytoskeletal reorganization and transcript profiles of vegetative profilins and Actin depolymerizing factors (ADFs) in Arabidopsis. *Acta Physiologiae Plantarum*, **38**, 1–4.

Finka, A., **Cuendet, A.F.H.**, **Maathuis, F.J.M.**, **Saidi, Y.** & **Goloubinoff, P.** (2012) Plasma membrane cyclic nucleotide gated calcium channels control land plant thermal sensing and acquired thermotolerance. *Plant Cell Online*, **24**, 3333–3348.

Finka, A., **Mattoo, R.U.H.** & **Goloubinoff, P.** (2016) Experimental milestones in the discovery of molecular chaperones as polypeptide unfolding enzymes. *Annual Review of Biochemistry*, **85**, 715–742.

Garagounis, C., **Kostaki, K.I.**, **Hawkins, T.J.**, **Cummins, I.**, **Fricker, M.D.**, **Hussey, P.J.** ***et al.*** (2017) Microcompartmentation of cytosolic aldolase by interaction with the Actin cytoskeleton in Arabidopsis. *Journal of Experimental Botany*, **68**, 885–898.

Gelová, Z., **Gallei, M.**, **Pernisová, M.**, **Brunoud, G.**, **Zhang, X.**, **Glanc, M.** ***et al.*** (2021) Developmental roles of auxin binding protein 1 in *Arabidopsis thaliana*. *Plant Science*, **303**, 110750.

Gonzalez-Jorge, S., **Ha, S.H.**, **Magallanes-Lundback, M.**, **Gilliland, L.U.**, **Zhou, A.**, **Lipka, A.E.** ***et al.*** (2013) Carotenoid cleavage dioxygenase4 is a negative regulator of β-carotene content in arabidopsis seeds. *Plant Cell*, **25**, 4812–4826.

Goyal, M. & **Asthir, B.** (2009) Polyamine catabolism influences antioxidative defense mechanism in shoots and roots of five wheat genotypes under high temperature stress. *Plant Growth Regulation*, **60**, 13–25.

Guihur, A., **Fauvet, B.**, **Finka, A.**, **Quadroni, M.** & **Goloubinoff, P.** (2020) Quantitative proteomic analysis to capture the role of heat-accumulated proteins in moss plant acquired thermotolerance. *Plant, Cell & Environment*, **44**, 2117–2133.

Guihur, A., **Rebeaud, M.E.** & **Goloubinoff, P.** (2022) How do plants feel the heat and survive? *Trends in Biochemical Sciences*, **47**, 824–838.

Halter, G., **Simonetti, N.**, **Suguitan, C.**, **Helm, K.**, **Soroksky, J.** & **Waters, E.R.** (2017) Patterns of thermotolerance, chlorophyll fluorescence, and heat shock gene expression vary among four Boechera species and *Arabidopsis thaliana*. *Botany*, **95**, 9–27.

Hamilton, E.W., III & **Heckathorn, S.A.** (2001) Mitochondrial adaptations to NaCl. Complex I is protected by anti-oxidants and small heat shock proteins, whereas complex II is protected by proline and betaine. *Plant Physiology*, **126**, 1266–1274.

Hatfield, J.L. & **Prueger, J.H.** (2015) Temperature extremes: effect on plant growth and development. *Weather and Climate Extremes*, **10**, 4–10.

Hayes, S., **Schachtschabel, J.**, **Mishkind, M.**, **Munnik, T.** & **Arisz, S.A.** (2020) Hot topic: Thermosensing in plants. *Plant, Cell & Environment*, **44**, 2018–2033.

Heckathorn, S.A., **Downs, C.A.** & **Coleman, J.S.** (1999) Small heat shock proteins protect electron transport in chloroplasts and mitochondria during stress. *American Zoologist*, **39**, 865–876.

Hooper, C.M., **Castleden, I.R.**, **Tanz, S.K.**, **Aryamanesh, N.** & **Millar, A.H.** (2017) SUBA4: the interactive data analysis centre for Arabidopsis subcellular protein locations. *Nucleic Acids Research*, **45**, 1064–1074.

Hooper, C.M., **Tanz, S.K.**, **Castleden, I.R.**, **Vacher, M.A.**, **Small, I.D.** & **Millar, A.H.** (2014) SUBAcon: a consensus algorithm for unifying the subcellular localization data of the Arabidopsis proteome. *Bioinformatics*, **30**, 3356–3364.

Hu, J.J., **Manduzio, S.**, **Kang, H.** ***et al.*** (2019) Mitochondrial small heat shock protein mediates seed germination via thermal sensing. *Proceedings of the National Academy of Sciences*, **116**, 4716–4721.

Huang, S., **Li, L.**, **Petereit, J.** & **Millar, A.H.** (2020) Protein turnover rates in plant mitochondria. *Mitochondrion*, **53**, 57–65.

Hüve, K., **Bichele, I.**, **Rasulov, B.** & **Niinemets, Ü.** (2011) When it is too hot for photosynthesis: heat-induced instability of photosynthesis in relation to respiratory burst, cell permeability changes and H_2O_2 formation. *Plant, Cell & Environment*, **34**, 113–126.

Jagadish, S.V.K., **Way, D.A.** & **Sharkey, T.D.** (2021) Plant heat stress: concepts directing future research. *Plant, Cell & Environment*, **44**, 1992–2005.

Jiang, H., **Liu, X.**, **Xiao, P.**, **Wang, Y.**, **Xie, Q.**, **Wu, X.** ***et al.*** (2023) Functional insights of plant bcl-2–associated ahanogene (BAG) proteins: multi-taskers in diverse cellular signal transduction pathways. *Frontiers in Plant Science*, **14**, 1136873.

Kabbage, M., **Kessens, R.**, **Bartholomay, L.C.** & **Williams, B.** (2017) The life and death of a plant cell. *Annual Review of Plant Biology*, **68**, 375–404.

Kan, Y., **Mu, X.-R.**, **Gao, J.**, **Lin, H.-X.** & **Lin, Y.** (2023) The molecular basis of heat stress responses in plants. *Molecular Plant*, **16**, 1612–1634.

Kang, C.H., **Lee, Y.M.**, **Park, J.H.**, **Nawkar, G.M.**, **Oh, H.T.**, **Kim, M.G.** ***et al.*** (2016) Ribosomal P3 protein AtP3B of Arabidopsis acts as both protein and RNA chaperone to increase tolerance of heat and cold stresses. *Plant, Cell & Environment*, **39**, 1631–1642.

Kaplan, F., **Kopka, J.**, **Haskell, D.W.**, **Zhao, W.**, **Schiller, K.C.**, **Gatzke, N.** ***et al.*** (2004) Exploring the temperature-sress metabolome of Arabidopsis. *Plant Physiology*, **136**, 4159–4168.

Kessner, D., **Chambers, M.**, **Burke, R.**, **Agus, D.** & **Mallick, P.** (2008) ProteoWizard: open source software for rapid proteomics tools development. *Bioinformatics*, **24**, 2534–2536.

Khan, A. & **Mathelier, A.** (2017) Intervene: a tool for intersection and visualization of multiple gene or genomic region sets. *BMC Bioinformatics*, **18**, 1–8.

Kosová, K., **Vítámvás, P.**, **Prášil, I.T.** & **Renaut, J.** (2011) Plant proteome changes under abiotic stress – contribution of proteomics studies to understanding plant stress response. *Journal of Proteomics*, **74**, 1301–1322.

Langella, O., **Valot, B.**, **Balliau, T.**, **Blein-Nicolas, M.**, **Bonhomme, L.** & **Zivy, M.** (2017) X!TandemPipeline: a tool to manage sequence redundancy for protein inference and phosphosite identification. *Journal of Proteome Research*, **16**, 494–503.

Larkindale, J. & **Vierling, E.** (2007) Core genome responses involved in acclimation to high temperature. *Plant Physiology*, **146**, 748–761.

Leck, M.A., **Simpson, R.L.** & **Thomas, V.** (2008) Why seedlings? In: Leck, M.A., Parker, V.T. & Simpson, R. (Eds.) *Seedling Ecology and Evolution*. Cambridge: Cambridge University Press, pp. 3–13.

Lee, K., **Lehmann, M.**, **Paul, M.V.**, **Wang, L.**, **Luckner, M.**, **Wanner, G.** ***et al.*** (2020) Lack of FIBRILLIN6 in *Arabidopsis thaliana* affects light acclimation and sulfate metabolism. *The New Phytologist*, **225**, 1715–1731.

Li, L., **Nelson, C.J.**, **Trösch, J.**, **Castleden, I.**, **Huang, S.** & **Millar, A.H.** (2017) Protein degradation rate in *Arabidopsis thaliana* leaf growth and development. *Plant Cell*, **29**, 207–228.

Li, L., **Xing, Y.**, **Chang, D.**, **Fang, S.**, **Cui, B.**, **Li, Q.** ***et al.*** (2016) CaM/BAG5/Hsc70 signaling complex dynamically regulates leaf senescence. *Scientific Reports*, **6**, 31889.

Liang, C., **Cheng, S.**, **Zhang, Y.**, **Sun, Y.**, **Fernie, A.R.**, **Kang, K.** ***et al.*** (2016) Transcriptomic, proteomic and metabolic changes in *Arabidopsis thaliana* leaves after the onset of illumination. *BMC Plant Biology*, **16**, 43.

Liberek, K., **Lewandowska, A.** & **Zietkiewicz, S.** (2008) Chaperones in control of protein disaggregation. *The EMBO Journal*, **27**, 328–335.

Lim, C.J., **Yang, K.A.**, **Hong, J.K.**, **Choi, J.S.**, **Yun, D.J.**, **Hong, J.C.** ***et al.*** (2006) Gene expression profiles during heat acclimation in *Arabidopsis thaliana*. *Journal of Plant Research*, **119**, 373–383.

Liu, H., **Able, A.J.** & **Able, J.A.** (2021) Priming crops for the future: rewiring stress memory. *Trends in Plant Science*, **27**, 699–716.

Logan, D.C. (2010) The dynamic plant chondriome. *Seminars in Cell & Developmental Biology*, **21**, 550–557.

Logan, D.C. & **Leaver, C.J.** (2000) Mitochondria-targeted GFP highlights the heterogeneity of mitochondrial shape, size and movement within living plant cells. *Journal of Experimental Botany*, **51**, 865–871.

Lv, W.T., **Lin, B.**, **Zhang, M.** & **Hua, X.J.** (2011) Proline accumulation is inhibitory to arabidopsis seedlings during heat stressspi. *Plant Physiology*, **156**, 1921–1933.

Maharjan, P.M., **Dilkes, B.P.**, **Fujioka, S.**, **Pěnčík, A.**, **Ljung, K.**, **Burow, M.** ***et al.*** (2014) Arabidopsis gulliver1/superroot2-7 identifies a metabolic basis for auxin and brassinosteroid synergy. *The Plant Journal*, **80**, 797–808.

Malerba, M., **Crosti, P.** & **Cerana, R.** (2010) Effect of heat stress on Actin cytoskeleton and endoplasmic reticulum of tobacco BY-2 cultured cells and its inhibition by Co2+. *Protoplasma*, **239**, 23–30.

Mathur, S., **Agrawal, D.** & **Jajoo, A.** (2014) Photosynthesis: response to high temperature stress. *Journal of Photochemistry and Photobiology. B*, **137**, 116–126.

Maziak, A., **Heidorn-Czarna, M.**, **Weremczuk, A.** & **Janska, H.** (2021) FTSH4 and OMA1 mitochondrial proteases reduce moderate heat stress-induced protein aggregation. *Plant Physiology*, **187**, 769–786.

McLoughlin, F., **Basha, E.**, **Fowler, M.E.**, **Kim, M.**, **Bordowitz, J.**, **Katiyar-Agarwal, S.** ***et al.*** (2016) Class I and II small heat shock proteins together with HSP101 protect protein translation factors during heat stress. *Plant Physiology*, **172**, 1221–1236.

Merret, R., **Carpentier, M.C.**, **Favory, J.J.**, **Picart, C.**, **Descombin, J.**, **Bousquet-Antonelli, C.** ***et al.*** (2017) Heat-shock protein HSP101 affects the release of ribosomal protein mRNAs for recovery after heat shock. *Plant Physiology*, **174**, 1216–1225.

Merret, R., **Nagarajan, V.K.**, **Carpentier, M.C.**, **Park, S.**, **Favory, J.J.**, **Descombin, J.** ***et al.*** (2015) Heat-induced ribosome pausing triggers mRNA co-translational decay in *Arabidopsis thaliana*. *Nucleic Acids Research*, **43**, 4121–4132.

Mittler, R., **Finka, A.** & **Goloubinoff, P.** (2012) How do plants feel the heat? *Trends in Biochemical*, **27**, 118–125.

Moran, R. (1982) Formulae for determination of chlorophyllous pigments extracted with N,N-dimethylformamide. *Plant Physiology*, **69**, 1376–1381.

Mounier, N. & **Arrigo, A.-P.** (2002) Actin cytoskeleton and small heat shock proteins: how do they interact? *Cell Stress & Chaperones*, **7**, 167–176.

Müller, J., **Menzel, D.** & **Šamaj, J.** (2007) Cell-type-specific disruption and recovery of the cytoskeleton in Arabidopsis thaliana epidermal root cells upon heat shock stress. *Protoplasma*, **230**, 231–242.

Nelson, B.K., **Cai, X.** & **Nebenfuhr, A.** (2007) A multicolored set of in vivo organelle markers for co-localization studies in Arabidopsis and other plants. *The Plant Journal*, **51**, 1126–1136.

Nguyen, C.C., **Nakaminami, K.**, **Matsui, A.**, **Kobayashi, S.**, **Kurihara, Y.**, **Toyooka, K.** ***et al.*** (2016) Oligouridylate binding protein 1b plays an integral role in plant heat stress tolerance. *Frontiers in Plant Science*, **7**, 853.

Niu, Y. & **Xiang, Y.** (2018) An overview of biomembrane functions in plant responses to high-temperature stress. *Frontiers in Plant Science*, **9**, 1–18.

Noël, L.D., **Cagna, G.**, **Stuttmann, J.**, **Wirthmüller, L.**, **Betsuyaku, S.**, **Witte, C.P.** ***et al.*** (2007) Interaction between SGT1 and cytosolic/nuclear HSC70 chaperones regulates Arabidopsis immune responses. *Plant Cell*, **19**, 4061–4076.

Obata, T. & **Fernie, A.R.** (2012) The use of metabolomics to dissect plant responses to abiotic stresses. *Cellular and Molecular Life Sciences*, **69**, 3225–3243.

Ohama, N., **Sato, H.**, **Shinozaki, K.** & **Yamaguchi-Shinozaki, K.** (2017) Transcriptional regulatory network of plant heat stress response. *Trends in Plant Science*, **22**, 53–65.

Oliveros, J. (2007) VENNY. An interactive tool for comparing lists with Venn diagrams. http://bioinfogp.cnb.csic.es/tools/venny/index.htm

Pan, R., **Jones, A.D.** & **Hu, J.** (2014) Cardiolipin-mediated mitochondrial dynamics and stress response in Arabidopsis. *Plant Cell Online*, **26**, 391–409.

Panikulangara, T.J., **Eggers-Schumacher, G.**, **Wunderlich, M.**, **Stransky, H.** & **Schöffl, F.** (2004) Galactinol synthase1. A novel heat shock factor target gene responsible for heat-induced synthesis of raffinose family oligosaccharides in Arabidopsis. *Plant Physiology*, **136**, 3148–3158.

Paszkiewicz, G., **Gualberto, J.M.**, **Benamar, A.**, **Macherel, D.** & **Logan, D.C.** (2017) Arabidopsis seed mitochondria are bioenergetically active immediately upon imbibition and specialize via biogenesis in preparation for autotrophic growth. *Plant Cell*, **29**, 109–128.

Pauwels, L., **Barbero, G.F.**, **Geerinck, J.**, **Tilleman, S.**, **Grunewald, W.**, **Pérez, A.C.** ***et al.*** (2010) NINJA connects the co-repressor TOPLESS to jasmonate signalling. *Nature*, **464**, 788–791.

Perez-Riverol, Y., **Bai, J.**, **Bandla, C.**, **García-Seisdedos, D.**, **Hewapathirana, S.**, **Kamatchinathan, S.** ***et al.*** (2022) The PRIDE database resources in 2022: a hub for mass spectrometry-based proteomics evidences. *Nucleic Acids Research*, **50**, D543–D552.

Perico, C. & **Sparkes, I.** (2018) Plant organelle dynamics: cytoskeletal control and membrane contact sites. *The New Phytologist*, **220**, 381–394.

Perkins-Kirkpatrick, S.E. & **Lewis, S.C.** (2020) Increasing trends in regional heatwaves. *Nature Communications*, **11**, 1–8.

Phillips, M.A., **D'Auria, J.C.**, **Gershenzon, J.** & **Pichersky, E.** (2008) The *Arabidopsis thaliana* type I isopentenyl diphosphate isomerases are targeted to multiple subcellular compartments and have overlapping functions in isoprenoid biosynthesis. *Plant Cell*, **20**, 677–696.

Posch, B.C., **Kariyawasam, B.C.**, **Bramley, H.**, **Coast, O.**, **Richards, R.A.**, **Reynolds, M.P.** ***et al.*** (2019) Exploring high temperature responses of photosynthesis and respiration to improve heat tolerance in wheat. *Journal of Experimental Botany*, **70**, 5051–5069.

Queitsch, C., **Hong, S.W.**, **Vierling, E.** & **Lindquist, S.** (2000) Heat shock protein 101 plays a crucial role in thermotolerance in Arabidopsis. *Plant Cell*, **12**, 479–492.

Réthoré, E., **D'Andrea, S.**, **Benamar, A.**, **Cukier, C.**, **Tolleter, D.**, **Limami, A.M.** ***et al.*** (2019) Arabidopsis seedlings display a remarkable resilience under severe mineral starvation using their metabolic plasticity to remain self-sufficient for weeks. *The Plant Journal*, **99**, 302–315.

Richter, K., **Haslbeck, M.** & **Buchner, J.** (2010) The heat shock response: life on the verge of death. *Molecular Cell*, **40**, 253–266.

Riedl, J., **Crevenna, A.H.**, **Kessenbrock, K.**, **Yu, J.H.**, **Neukirchen, D.**, **Bista, M.** ***et al.*** (2008) Lifeact: a versatile marker to visualize F-Actin. *Nature Methods*, **5**, 605–607.

Rohart, F., **Gautier, B.**, **Singh, A.** & **Lê Cao, K.-A.** (2017) mixOmics: an R package for 'omics feature selection and multiple data integration D. Schneidman, ed. *PLoS Computational Biology*, **13**, e1005752.

Ruelland, E. & **Zachowski, A.** (2010) How plants sense temperature. *Environmental and Experimental Botany*, **69**, 225–232.

Saidi, Y., **Finka, A.** & **Goloubinoff, P.** (2011) Heat perception and signalling in plants: a tortuous path to thermotolerance. *The New Phytologist*, **190**, 556–565.

Sapir-Mir, M., **Mett, A.**, **Belausov, E.**, **Tal-Meshulam, S.**, **Frydman, A.**, **Gidoni, D.** ***et al.*** (2008) Peroxisomal localization of arabidopsis isopentenyl diphosphate isomerases suggests that part of the plant isoprenoid mevalonic acid pathway is compartmentalized to peroxisomes. *Plant Physiology*, **148**, 1219–1228.

Scafaro, A.P., **Fan, Y.**, **Posch, B.C.**, **Garcia, A.**, **Coast, O.** & **Atkin, O.K.** (2021) Responses of leaf respiration to heatwaves. *Plant, Cell & Environment*, **44**, 2090–2101.

Schindelin, J., **Arganda-Carreras, I.**, **Frise, E.**, **Kaynig, V.**, **Longair, M.**, **Pietzsch, T.** ***et al.*** (2012) Fiji: an open-source platform for biological-image analysis. *Nature Methods*, **9**, 676–682.

Scott, I. & **Logan, D.C.** (2008) Mitochondrial morphology transition is an early indicator of subsequent cell death in Arabidopsis. *The New Phytologist*, **177**, 90–101.

Serrano, N., **Ling, Y.**, **Bahieldin, A.** & **Mahfouz, M.M.** (2019) Thermopriming reprograms metabolic homeostasis to confer heat tolerance. *Scientific Reports*, **9**, 1–14.

Sharma, M., **Banday, Z.Z.**, **Shukla, B.N.** & **Laxmi, A.** (2019) Glucose-regulated HLP1 acts as a key molecule in governing thermomemory. *Plant Physiology*, **180**, 1081–1100.

Shoemaker, C.J. & **Green, R.** (2012) Translation drives mRNA quality control. *Nature Structural & Molecular Biology*, **19**, 594–601.

Siddique, M., **Gernhard, S.**, **Von Koskull-Döring, P.**, **Vierling, E.** & **Scharf, K.D.** (2008) The plant sHSP superfamily: five new members in *Arabidopsis thaliana* with unexpected properties. *Cell Stress & Chaperones*, **13**, 183–197.

Song, J., **Liu, Q.**, **Hu, B.** & **Wu, W.** (2016) Comparative transcriptome profiling of Arabidopsis Col-0 in responses to heat stress under different light conditions. *Plant Growth Regulation*, **79**, 209–218.

Stupnikova, I., **Benamar, A.**, **Tolleter, D.**, **Grelet, J.**, **Borovskii, G.**, **Dorne, A.-J.** ***et al.*** (2006) Pea seed mitochondria are endowed with a remarkable tolerance to extreme physiological temperatures. *Plant Physiology*, **140**, 326–335.

Sun, A.-Z. & **Guo, F.-Q.** (2016) Chloroplast retrograde regulation of heat stress responses in plants. *Frontiers in Plant Science*, **7**, 398.

Szklarczyk, D., **Gable, A.L.**, **Lyon, D.**, **Junge, A.**, **Wyder, S.**, **Huerta-Cepas, J.** ***et al.*** (2019) STRING v11: protein–protein association networks with increased coverage, supporting functional discovery in genome-wide experimental datasets. *Nucleic Acids Research*, **47**, D607–D613.

Tian, T., **Liu, Y.**, **Yan, H.**, **You, Q.**, **Yi, X.**, **Du, Z.** ***et al.*** (2017) AgriGO v2.0: a GO analysis toolkit for the agricultural community, 2017 update. *Nucleic Acids Research*, **45**, W122–W129.

Tomaštíková, E., **Cenklová, V.**, **Kohoutová, L.**, **Petrovská, B.**, **Váchová, L.**, **Halada, P.** ***et al.*** (2012) Interactions of an Arabidopsis RanBPM homologue with LisH-CTLH domain proteins revealed high conservation of CTLH complexes in eukaryotes. *BMC Plant Biology*, **12**, 83.

Török, Z., **Goloubinoff, P.**, **Horváth, I.**, **Tsvetkova, N.M.**, **Glatz, A.**, **Balogh, G.** ***et al.*** (2001) Synechocystis HSP17 is an amphitropic protein that stabilizes heat-stressed membranes and binds denatured proteins for subsequent chaperone-mediated refolding. *Proceedings of the National Academy of Sciences*, **98**(6), 3098–3103.

Tsukimoto, R., **Isono, K.**, **Kajino, T.**, **Iuchi, S.**, **Shinozawa, A.**, **Yotsui, I.** ***et al.*** (2022) Mitochondrial fission complex is required for long-term heat tolerance of Arabidopsis. *Plant & Cell Physiology*, **63**, 296–304.

Tzin, V. & **Galili, G.** (2010) New insights into the shikimate and aromatic amino acids biosynthesis pathways in plants. *Molecular Plant*, **3**, 956–972.

Valot, B., **Langella, O.**, **Nano, E.** & **Zivy, M.** (2011) MassChroQ: a versatile tool for mass spectrometry quantification. *Proteomics*, **11**, 3572–3577.

Van Gestel, K., **Kohler, R.H.** & **Verbelen, J.P.** (2002) Plant mitochondria move on F-Actin, but their positioning in the cortical cytoplasm depends on both F-Actin and microtubules. *Journal of Experimental Botany*, **53**, 659–667.

Volkov, R.A., **Panchuk, I.I.**, **Mullineaux, P.M.** & **Schöffl, F.** (2006) Heat stress-induced H_2O_2 is required for effective expression of heat shock genes in Arabidopsis. *Plant Molecular Biology*, **61**, 733–746.

Wahid, A., **Gelani, S.**, **Ashraf, M.** & **Foolad, M.R.** (2007) Heat tolerance in plants: An overview. *Environmental and Experimental Botany*, **61**, 199–223.

Wang, L., **Ma, K.-B.**, **Lu, Z.-G.**, **Ren, S.-X.**, **Jiang, H.-R.**, **Cui, J.-W.** ***et al.*** (2020) Differential physiological, transcriptomic and metabolomic responses of Arabidopsis leaves under prolonged warming and heat shock. *BMC Plant Biology*, **20**(1), 86.

Wang, Q.-L., **Chen, J.-H.**, **He, N.-Y.** & **Guo, F.-Q.** (2018) Metabolic reprogramming in chloroplasts under heat stress in plants. *International Journal of Molecular Sciences*, **19**, 849.

Waters, E.R. (2013) The evolution, function, structure, and expression of the plant sHSPs. *Journal of Experimental Botany*, **64**, 391–403.

Waters, E.R. & **Vierling, E.** (2020) Plant small heat shock proteins – evolutionary and functional diversity. *The New Phytologist*, **227**, 24–37.

Weber, C., **Nover, L.** & **Fauth, M.** (2008) Plant stress granules and mRNA processing bodies are distinct from heat stress granules. *The Plant Journal*, **56**, 517–530.

Yamori, W., **Hikosaka, K.** & **Way, D.A.** (2014) Temperature response of photosynthesis in C3, C4, and CAM plants: temperature acclimation and temperature adaptation. *Photosynthesis Research*, **119**, 101–117.

Yángüez, E., **Castro-Sanz, A.B.**, **Fernández-Bautista, N.**, **Oliveros, J.C.** & **Castellano, M.M.** (2013) Analysis of genome-wide changes in the translatome of Arabidopsis seedlings subjected to heat stress. *PLoS One*, **8**, e71425.

Yuenyong, W., **Sirikantaramas, S.**, **Qu, L.-J.** & **Buaboocha, T.** (2019) Isocitrate lyase plays important roles in plant salt tolerance. *BMC Plant Biology*, **19**, 472.

Zampieri, M., **Ceglar, A.**, **Dentener, F.** & **Toreti, A.** (2017) Wheat yield loss attributable to heat waves, drought and water excess at the global, national and subnational scales. *Environmental Research Letters*, **12**, 064008.

Zhang, A., **Jiang, X.**, **Zhang, F.**, **Wang, T.** & **Zhang, X.** (2020) Dynamic response of RNA editing to temperature in grape by RNA deep sequencing. *Functional & Integrative Genomics*, **20**, 421–432.

Zhang, B., **Fan, Y.**, **Cao, P.** & **Tan, K.** (2021) Multifaceted roles of HSF1 in cell death: a state-of-the-art review. *Biochimica et Biophysica Acta (BBA)-Reviews on Cancer*, **1876**, 188591.

Zhang, J.X., **Wang, C.**, **Yang, C.Y.**, **Wang, J.Y.**, **Chen, L.**, **Bao, X.M.** ***et al.*** (2010) The role of Arabidopsis AtFes1A in cytosolic Hsp70 stability and abiotic stress tolerance. *The Plant Journal*, **62**, 539–548.

Zhang, L., **Duan, Z.**, **Zhang, J.** & **Peng, L.** (2016) Biogenesis factor required for ATP synthase 3 facilitates assembly of the chloroplast ATP synthase complex. *Plant Physiology*, **171**, 1291–1306.

Zhang, N., **Belsterling, B.**, **Raszewski, J.** & **Tonsor, S.J.** (2015) Natural populations of *Arabidopsis thaliana* differ in seedling responses to high temperature stress. *AoB Plants*, **7**, plv101.

Zhang, X., **Carter, M.S.**, **Vetting, M.W.**, **San Francisco, B.**, **Zhao, S.**, **al-Obaidi, N.F.** ***et al.*** (2016) Assignment of function to a domain of unknown function: DUF1537 is a new kinase family in catabolic pathways for acid sugars. *Proceedings of the National Academy of Sciences of the United States of America*, **113**, E4161–E4169.

Zhong, L., **Zhou, W.**, **Wang, H.**, **Ding, S.**, **Lu, Q.**, **Wen, X.** ***et al.*** (2013) Chloroplast small heat shock protein HSP21 interacts with plastid nucleoid protein pTAC5 and is essential for chloroplast development in arabidopsis under heat stress. *Plant Cell*, **25**, 2925–2943.